The parasite *Toxoplasma* sequesters diverse Rab host vesicles within an intravacuolar network

Julia D. Romano,[1] Sabrina J. Nolan,[1] Corey Porter,[1] Karen Ehrenman,[1] Eric J. Hartman,[1] Ru-ching Hsia,[2] and Isabelle Coppens[1]

[1]Department of Molecular Microbiology and Immunology, Johns Hopkins University Bloomberg School of Public Health, Baltimore, MD
[2]Electron Microscopy Core Imaging Facility, University of Maryland Baltimore, Baltimore, MD

Many intracellular pathogens subvert host membrane trafficking pathways to promote their replication. *Toxoplasma* multiplies in a membrane-bound parasitophorous vacuole (PV) that interacts with mammalian host organelles and intercepts Golgi Rab vesicles to acquire sphingolipids. The mechanisms of host vesicle internalization and processing within the PV remain undefined. We demonstrate that *Toxoplasma* sequesters a broad range of Rab vesicles into the PV. Correlative light and electron microscopy analysis of infected cells illustrates that intravacuolar Rab1A vesicles are surrounded by the PV membrane, suggesting a phagocytic-like process for vesicle engulfment. Rab11A vesicles concentrate to an intravacuolar network (IVN), but this is reduced in *Δgra2* and *Δgra2Δgra6* parasites, suggesting that tubules stabilized by the TgGRA2 and TgGRA6 proteins secreted by the parasite within the PV contribute to host vesicle sequestration. Overexpression of a phospholipase TgLCAT, which is localized to the IVN, results in a decrease in the number of intravacuolar GFP-Rab11A vesicles, suggesting that TgLCAT controls lipolytic degradation of Rab vesicles for cargo release.

Introduction

Membrane trafficking pathways mediate many aspects of cellular physiology, including endocytosis, transport of cargo, regulation of metabolism, signaling, and immunity and, therefore, are often targeted and subverted by intracellular pathogens (Saka and Valdivia, 2010; Asrat et al., 2014). Among them, the human parasite *Toxoplasma gondii* exploits host endocytic and secretory trafficking pathways that transport lipids contributing to parasite development (Coppens et al., 2006; Romano et al., 2013).

Bypassing the phagocytic pathway, *Toxoplasma* actively invades mammalian cells, creating a membrane-bound compartment, the parasitophorous vacuole (PV). The PV resists fusion with the host degradative endolysosomal system (Clough and Frickel, 2017), thereby protecting the parasite from host cytolytic factors. The unique biochemical properties of the PV result from the modification of the PV membrane (PVM) and lumen by proteins and lipids secreted by *Toxoplasma* (Sibley, 2011; Clough and Frickel, 2017; Hakimi et al., 2017). Further modifications include the creation of proteinaceous pores inserted within the PVM, which allow the passage of small solutes (Schwab et al., 1994; Gold et al., 2015), and the presence of membranous tubules that form an intravacuolar network (IVN; Sibley et al., 1995). Secreted by the parasite into the PV, the IVN is stabilized by two tubulogenic proteins, TgGRA2 and TgGRA6 (Mercier et al., 2002; Cesbron-Delauw et al., 2008; Travier et al., 2008), and further expanded with host lipids salvaged by the parasite (Caffaro and Boothroyd, 2011).

Toxoplasma modifies its host cell as it alters signaling pathways (e.g., STAT) by secreting effectors that modulate pathway components, activate transcription factors, and induce small noncoding RNAs (Hakimi et al., 2017) and, despite the nonfusogenic nature of its PV, it reorganizes many host structures/organelles. For example, the microtubule-organizing center relocalizes to the PV, which is then encased by microtubules (Melo et al., 2001; Coppens et al., 2006; Romano et al., 2008; Walker et al., 2008), the ER and mitochondria attach to the PV (de Melo et al., 1992; Melo and de Souza, 1997; Sinai et al., 1997; Pernas and Boothroyd, 2010), with the latter interaction mediated by the parasite effector MAF1 (Pernas et al., 2014), and endocytic organelles and the Golgi concentration around the PV, where the Golgi fragments into ministacks (Coppens et al., 2006; Romano et al., 2013). The parasite is auxotrophic for many metabolites (Blader and Koshy, 2014; Coppens, 2014), and its intracellular survival depends on its ability to retrieve nutrients from the host cell. In fact, the parasite scavenges

Correspondence to Isabelle Coppens: icoppens@jhsph.edu; Julia D. Romano: jromano2@jhu.edu

Abbreviations used: CLEM, correlative light and electron microscopy; HFF, human foreskin fibroblast; IFA, immunofluorescence assay; IVN, intravacuolar network; LDL, low-density lipoprotein; MOC, Mander's overlap coefficient; OA, oleic acid; PCC, Pearson's correlation coefficient; PPM, parasite plasma membrane; PV, parasitophorous vacuole; PVM, PV membrane; PVMP, PVM projections; TEM, transmission electron microscopy.

© 2017 Romano et al. This article is distributed under the terms of an Attribution–Noncommercial–Share Alike–No Mirror Sites license for the first six months after the publication date (see http://www.rupress.org/terms/). After six months it is available under a Creative Commons License (Attribution–Noncommercial–Share Alike 4.0 International license, as described at https://creativecommons.org/licenses/by-nc-sa/4.0/).

The Rockefeller University Press
J. Cell Biol. Vol. 216 No. 12 4235–4254
https://doi.org/10.1083/jcb.201701108

THE JOURNAL OF CELL BIOLOGY

Downloaded from http://rupress.org/jcb/article-pdf/216/12/4235/1597780/jcb_201701108.pdf by guest on 05 December 2025

cholesterol from host endolysosomes by internalizing these structures into the PV (Coppens et al., 2006). The parasite also salvages sphingolipids from the host Golgi (de Melo and de Souza, 1996; Romano et al., 2013) by sequestering Golgi-derived Rab GTPases (Rab14, Rab30, and Rab43) into the PV. Expression of dominant-negative Rab14 and Rab43 results in reduced host-derived sphingolipids in the PV (Romano et al., 2013), highlighting the physiological relevance of the cooption of host Rab vesicular trafficking pathways by *Toxoplasma*, in part for access to nutrients.

Because host endolysosomes and Rab vesicles are sequestered within the PV as intact structures, this raises perplexing questions of how these structures are internalized into the PV without fusion with the PVM and how they are processed in the PV to release their content. In this study, we followed different host Rabs to pinpoint the host trafficking pathways intercepted by the PV, and we used host GFP-Rab proteins to probe the role of parasite proteins associated with the IVN in host vesicle internalization and processing.

Results

Toxoplasma intercepts multiple intracellular trafficking pathways in the host cell

Toxoplasma scavenges host lipids from endolysosomes (Coppens et al., 2006) and Golgi-derived vesicles (Romano et al., 2013), effectively diverting host intracellular trafficking pathways. To pinpoint areas of interception between the PV and host trafficking circuits, we monitored the distribution of host Rab GTPases in infected cells, as these proteins are involved in the transport and fusion of vesicles from distinct trafficking pathways. To exclusively track the movement of host (not parasite) Rab vesicles in infected cells, we ectopically expressed GFP-tagged Rab constructs in mammalian cells and then infected with *Toxoplasma*. The localization of the GFP-Rab proteins in infected cells was monitored by fluorescence microscopy by collecting a series of optical z-sections throughout the PV.

We investigated the localization of several Rab proteins involved in the exocytic, retrograde, recycling, endocytic, and autophagosomal pathways (Table 1 and Fig. S1). GFP-Rab foci were observed within the PV for each Rab construct but with some selectivity. The percentage of the PV population with intra-PV foci varied among Rabs, as more than 80% of PVs contained Rabs involved in vesicle trafficking from endosomes to the plasma membrane (Rab4A, Rab11A, and Rab11B), from the ER to the Golgi (Rab1A), from the Golgi to the plasma membrane (Rab10, Rab14), and in the autophagosomal pathway (Rab24). Rabs involved in retrograde trafficking (Rab6A and Rab9A) were detected in the PV the least. Furthermore, the attribute of the intra-PV GFP-Rab foci varied. Many bright intra-PV foci were observed for Rab1A, Rab10, Rab11A, Rab11B, and Rab24 (Figs. 1 and S1), whereas fewer bright intra-PV Rab2A, Rab4A, Rab5A, and Rab7A foci were detected. Typically, only a few faint foci were observed for Rab6A and Rab9A (Fig. S1). These findings reveal the remarkable ability of *Toxoplasma* to reroute many host trafficking pathways to its PV to sequester specific Rab-derived vesicles or fragments within the lumen.

We extended these studies to the pathogen *Neospora caninum*, an apicomplexan parasite closely related to *Toxoplasma* with whom it shares many intracellular features, including the recruitment of host organelles at the PV (Nolan et al., 2015). By tracking the distribution of host GFP-Rab proteins in *N. caninum*–infected cells, we also observed Rab proteins in the PV of *N. caninum*; however, fewer *N. caninum* PVs contained Rab foci compared with *Toxoplasma* (Table 1). This observation highlights the similar properties of *Toxoplasma* and *N. caninum* PVs, as the two parasites are proficient in hijacking several host cellular trafficking pathways.

Next, we monitored the temporal distribution of host GFP-Rab1A in *Toxoplasma*-infected cells (Fig. S2 A). By the time the parasite underwent its first round of replication (~8 h after infection), host GFP-Rab1A partially surrounded the PV, and this perivacuolar association was maintained throughout infection. In some PVs with two parasites, we detected intra-PV GFP-Rab1A foci squeezed between the parasites. As the number of parasites within the PV increased, we observed a greater number of GFP-Rab1A foci in the PV (Fig. S2 A). In PVs with 8 to 16 parasites, there were often multiple, bright GFP-Rab1A foci, localized predominantly in the middle of the PV, near the basal end of the parasites, which are arranged in a rosette structure.

To ensure that the intra-PV foci represent host GFP-Rab proteins and not GFP alone, we confirmed the intra-PV localization of Rab proteins using immunofluorescence assays (IFAs) and anti-Rab antibodies. We generated a VERO cell line stably expressing GFP-Rab11A, infected with parasites, and probed with antibodies against Rab11. In uninfected cells, the localization of the GFP and Rab11 signals strongly correlated with a Pearson's correlation coefficient (PCC) of 0.766 and Mander's overlap coefficients (MOC) of 0.973 and 0.81 for the GFP and Rab11 channels, respectively (Fig. 1 A). The anti-Rab11 antibody cross-reacted with the parasite's Rab11 protein; however, by examining host GFP foci localized within the PV lumen, we detected foci that were costained for both GFP and Rab11 with a PCC of 0.66 and MOCs of 0.722 and 0.454 for the GFP and Rab11 channels, respectively; the lower MOC value in Fig. 1 for the Rab11 channel was expected, as the antibodies also recognized the parasite's Rab11. Many GFP- and Rab11-positive foci accumulated in the middle of the PV (Fig. 1 A, positive product of the difference of the means), demonstrating unequivocally that the intra-PV host GFP foci retained Rab11.

To exclude any mislocalization of host Rab vesicles caused by the exogenous expression of GFP-Rab proteins, we performed IFA using anti–Rab11 antibodies to visualize Rab11 in HeLa cells infected for 24 h (Fig. 1 B). As in our transfection assays, we detected Rab11 foci within the PV lumen, establishing that the internalization was not artifactually induced by overexpression of Rab proteins. These data were further confirmed by monitoring by IFA the distribution of other endogenous organellar markers such as LIMP1/LAMP3/CD63 (LIMP), a protein of multivesicular bodies (Kobayashi et al., 2000), and lysobisphosphatidic acid, a unique lipid of multivesicular bodies (Kobayashi et al., 1998), for which a fluorescent signal was similarly apparent within the PV (Fig. S2, B and C).

To address the specificity of the PV for host membranes associated with the Rab family of small GTPases, we examined the distribution of the Ras family of small GTPases. In infected cells, we observed GFP-KRas4B predominantly on the host plasma membrane and to a lesser extent on intracellular vesicles. We did not detect GFP-KRas4B–containing structures within the PV (Fig. S2 D). Similar results were obtained for NRas, HRas, and KRas4A (not depicted).

Downloaded from http://rupress.org/jcb/article-pdf/216/12/4235/1597780/jcb_201701108.pdf by guest on 05 December 2025

Because Rab effector proteins regulate the transport and targeting of Rab vesicles to their target membranes, we examined the role of the Rab1 tethering factor p115/Uso1p in targeting Rab1 to the PV; p115/Uso1p binds specifically to GTP-bound Rab1 and participates in multiple stages of ER/Golgi transport (Allan et al., 2000; Moyer et al., 2001; Beard et al., 2005). In infected cells, the GFP-p115 signal partially surrounded the PV but was not detected inside the PV or on the PVM (Fig. S2 E), suggesting that p115 does not mediate the PV–Rab1 interaction. Furthermore, components of host trafficking pathways are not indiscriminately targeted by the parasite.

The GTP-bound form of host Rab proteins is predominantly observed within the PV

In their GTP-bound form, Rab GTPases recruit specific sets of effector proteins onto membranes (Zhen and Stenmark, 2015). To determine whether the GTPase activity of Rab is required for PV internalization (i.e., whether the Rab foci observed in the PV lumen correspond to Rab vesicles and not Rab protein aggregates), we expressed Rab1A GTP-locked (Q70L) and Rab1A GDP-locked (S25N) mutants and compared their localization to WT Rab1A in infected cells (Fig. 1 C); GFP-Rab1A localized to ER–Golgi compartments in uninfected cells (Fig. 1 D). In WT and the GTP-locked mutant, we observed multiple, bright GFP-Rab1A foci inside the PV (Fig. 1 C). GFP-Rab1A foci were detected in 90% and 100% of PVs with either 8 or 16 parasites, respectively (Fig. 1 E). GTP-locked GFP-Rab1A foci were observed in all PVs (8 and 16 parasites), whereas GDP-locked GFP-Rab1A foci were only detected in 9% or 26% of PVs with either 8 or 16 parasites, respectively (Fig. 1 E). Furthermore, the staining pattern of intra-PV GFP-Rab1A S25N was less bright and more diffuse than the pattern observed for WT or the GTP-locked mutant, which both had bright, clearly defined foci (Fig. 1 C). These results suggest that the GTP-bound form of Rab1A was preferentially internalized into the PV, indicating that Rab1A foci are mostly bona fide vesicles.

Host GFP-Rab vesicles are surrounded by a membrane within the PV

To determine whether the GFP-Rab foci denote host vesicles encased within the PV, we used correlative light and electron microscopy (CLEM) and immunogold staining to examine the ultrastructure of intravacuolar Rab foci in greater detail.

For CLEM analysis, HeLa cells expressing GFP-Rab1A were infected with RFP-expressing *Toxoplasma* for 24 h and viewed by fluorescence microscopy to identify PVs containing GFP-Rab1A foci (Fig. S3). Then, the samples were processed for EM, and the same PVs were viewed for ultrastructural analysis. We selected GFP-Rab1A foci located near the inside edge of the PVM (Fig. 2, A and B), near the edge of a parasite (Fig. 2 A), and in the middle of the PV (Fig. 2 B). In each case, the GFP-Rab1A foci corresponded to a membrane-bound structure that was encased in another membrane (Fig. 2, A, B1, and B2, arrowheads). These structures were reminiscent of intra-PV host low-density lipoprotein (LDL)–containing endosomes that were also surrounded by a membrane, likely the PVM (Coppens et al., 2006; Fig. 2 C).

For the GFP-Rab1A foci in the center of the PV (Fig. 2 B2) and near the PVM (Fig. 2 A1), we observed multiple double-membrane vesicles in close proximity, with the inner

Table 1. **Host GFP-Rab internalized by the PV of *Toxoplasma* and *N. caninum***

GFP-Rab GTPase	Site of action (references)	Percentage of PVs with internalized GFP-Rab	
		Toxoplasma	*N. caninum*
Rab1A	ER–Golgi (anterograde); intra-Golgi; IC-PM (Plutner et al., 1991; Tisdale et al., 1992; Moyer et al., 2001; Sannerud et al., 2006)	95%	33%
Rab2A	ER–Golgi (retrograde; Tisdale et al., 1992; Tisdale and Balch, 1996; Tisdale, 1999)	67%	nd
Rab4A	EE-PM (fast; van der Sluijs et al., 1992; Daro et al., 1996; Vollenweider et al., 1997; McCaffrey et al., 2001)	83%	nd
Rab5A	PM-EE (EE formation; Gorvel et al., 1991; Bucci et al., 1992; Stenmark et al., 1994)	67%	nd
Rab6A	ER–Golgi; intra-Golgi; EE-TGN (Martinez et al., 1994; Girod et al., 1999; White et al., 1999; Mallard et al., 2002)	46%	nd
Rab7A	EE-LE (EE maturation); LE-lysosome (Feng et al., 1995; Méresse et al., 1995; Vitelli et al., 1997; Press et al., 1998)	62%	22%
Rab9A	LE-TGN (Lombardi et al., 1993; Riederer et al., 1994)	58%	nd
Rab10	Vesicles to PM; ER structure/dynamics (Babbey et al., 2006; Sano et al., 2007, 2008; Schuck et al., 2007; Wang et al., 2010; Chen and Lippincott-Schwartz, 2013; English and Voeltz, 2013)	90%	nd
Rab11A	RE-PM (slow); EE-TGN; TGN-PM; cytokinesis (Ullrich et al., 1996; Chen et al., 1998; Ren et al., 1998; Wilcke et al., 2000; Horgan et al., 2004; Wilson et al., 2005)	89%	31%
Rab11B	RE-PM (slow); EE-TGN; TGN-PM (Schlierf et al., 2000; Silvis et al., 2009; Butterworth et al., 2012)	100%	38%
Rab14	TGN-endosomes; TGN-apical PM (Junutula et al., 2004; Kitt et al., 2008)	94%	29%
Rab24	Autophagosome maturation/clearance; cell division (Munafó and Colombo, 2002; Militello et al., 2013; Ylä-Anttila et al., 2015)	91%	31%
Rab30	Golgi morphology (Kelly et al., 2012)	75%	21%
Rab43	ER–Golgi (Haas et al., 2007; Dejgaard et al., 2008)	68%	2%

HeLa cells were transiently transfected with GFP-Rab constructs and then infected with *Toxoplasma* or *N. caninum* for 24–32 h. The percentage of PVs with intravacuolar foci was determined as described in Materials and methods. Number of PVs: 19–28. EE, early endosome; IC, intermediate compartment; LE, late endosome; nd, not determined; PM, plasma membrane; RE, recycling endosome.

Downloaded from http://rupress.org/jcb/article-pdf/216/12/4235/1597780/jcb_201701108.pdf by guest on 05 December 2025

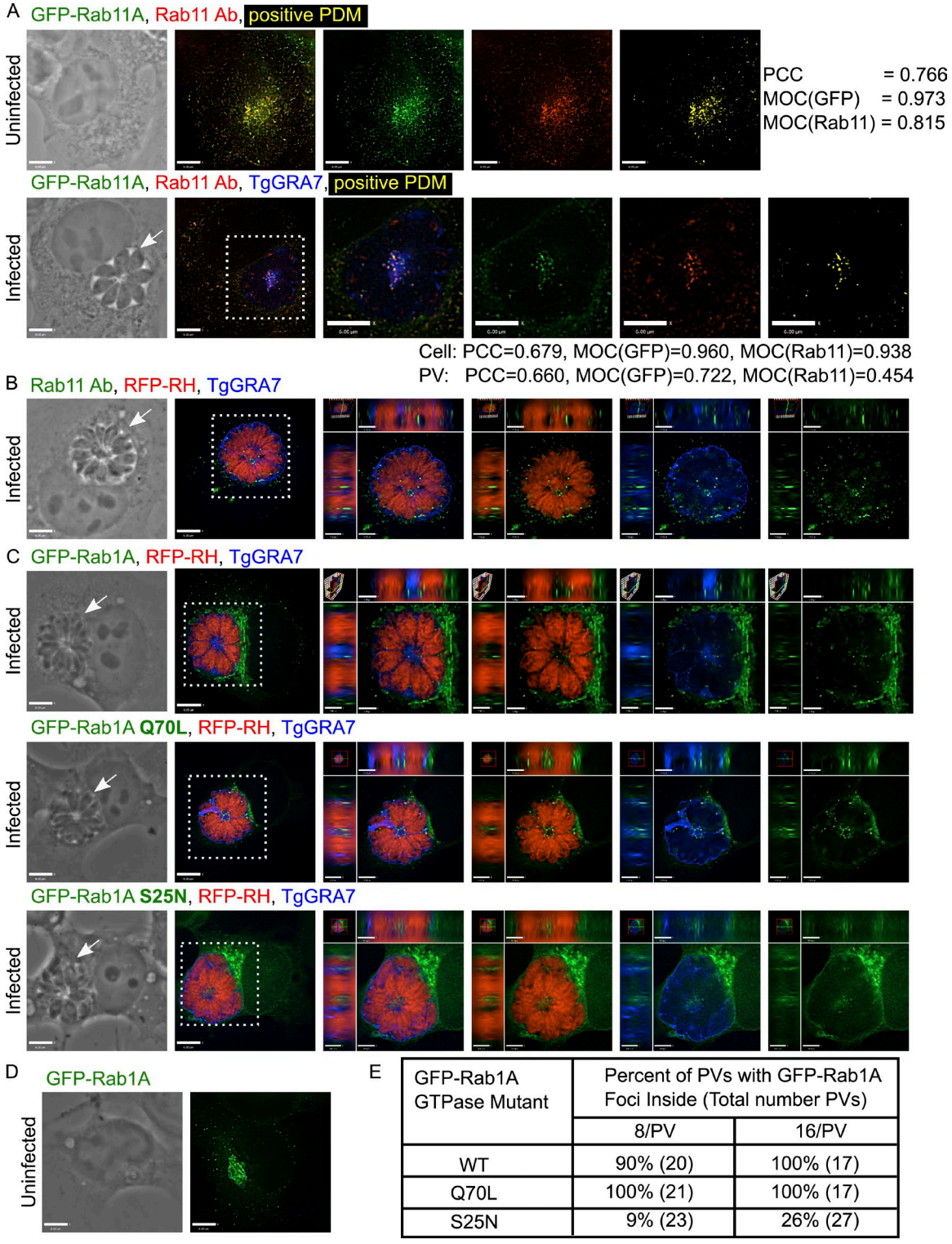

E

GFP-Rab1A GTPase Mutant	Percent of PVs with GFP-Rab1A Foci Inside (Total number PVs)	
	8/PV	16/PV
WT	90% (20)	100% (17)
Q70L	100% (21)	100% (17)
S25N	9% (23)	26% (27)

Figure 1. **Analysis of host Rab11 and Rab1A foci in the PV.** (A) VERO cells expressing GFP-Rab11A (green) were infected with parasites for 24 h and immunostained for Rab11 (red) and TgGRA7 (blue). To measure the level of colocalization, a positive product of the difference of the means (PDM; yellow) was calculated for uninfected and infected cells with PCC and MOC for the GFP and Rab11 channels. (B) VERO cells infected with RFP expressing parasites for 24 h (RFP-RH; red) were immunostained for Rab11 (green) and TgGRA7 (blue). (C) HeLa cells expressing GFP-Rab1A, the GTP-locked mutant Q70L, or the GDP-locked mutant S25N (green) were infected with RFP-RH for 24 h (16 parasites/PV) and immunostained for TgGRA7 (blue). (D) An uninfected, GFP-Rab1A expressing HeLa cell shows Rab1A in the ER–Golgi. (E) Percentage of PVs containing intra-PV GFP-Rab1A foci for one representative experiment. For all images, individual z-slices are shown; the boxed region is magnified in the orthogonal views, highlighting the PV (arrows). Bars: 6 µm; (orthogonal views) 1.7 µm.

Downloaded from http://rupress.org/jcb/article-pdf/216/12/4235/1597780/jcb_201701108.pdf by guest on 05 December 2025

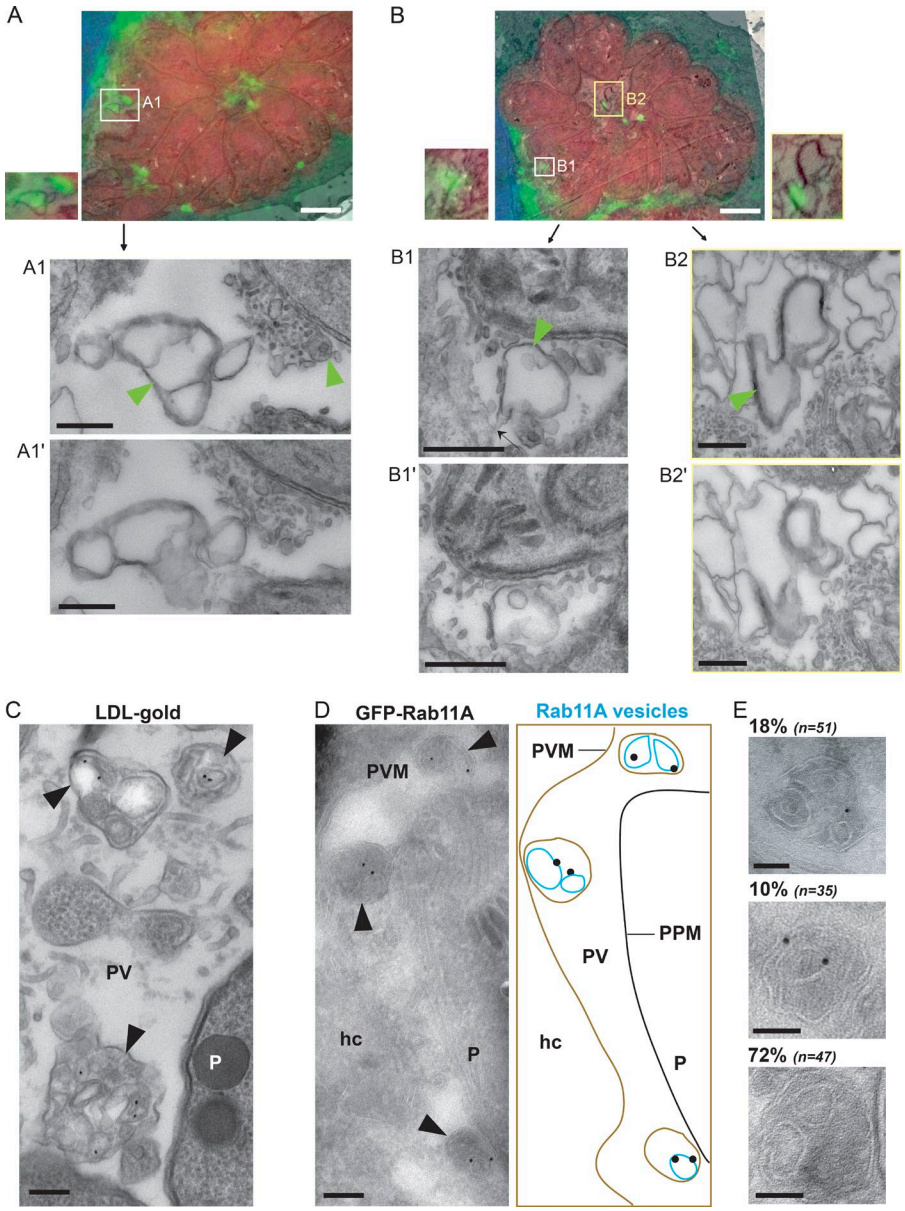

Figure 2. **Morphology of intra-PV host vesicles.** (A and B) HeLa cells transiently transfected with GFP-Rab1A (green) were infected with RFP-RH for 24 h, stained with DAPI (blue), and processed for CLEM. An overlay of a fluorescent image with its corresponding EM image is shown for two different PVs. Magnified EM serial sections of the boxed regions are shown (A1 and A1′, B1 and B1′, and B2 and B2′; bars, 100 nm). Black arrow in B1 shows attachment point of the vesicles to the PVM. Structures corresponding to the GFP-Rab1A foci are indicated with green arrowheads. Bars, 500 nm. (C) Infected VERO cells were incubated with LDL adsorbed to gold particles for 20 h and processed for TEM. Intra-PV structures containing gold particles are indicated with black arrowheads. Bar, 100 nm. (D) Infected (24 h), GFP-Rab11A–expressing VERO cells were immunogold labeled with antibodies to GFP. Arrowheads indicate GFP-Rab11A vesicles. The diagram corresponds to the immuno-EM image with host GFP-Rab11A vesicles (blue), the PVM (brown), and the parasite's plasma membrane (PPM; black). Bar, 100 nm. (E) Distribution of intra-PV structures containing vesicles unlabeled or single or double labeled with gold particles. Bars, 50 nm. hc, host cell; P, parasite.

vesicles corresponding to the membrane of GFP-Rab1A foci. The GFP-Rab1A focus located near the parasite (Fig. 2 A1), also corresponded to a vesicle encased in a membrane though the structure was smaller, appeared to contain a single vesicle and was found in a region of electron-dense material consisting of tubules and membrane-bounded structures, along the edge of the parasite's plasma membrane. The second GFP-Rab1A focus located near the PVM (Fig. 2 B1) corresponded to a vesicle enclosed in a membrane (PPM), but the outer membrane surrounding the vesicle appeared to be connected to the PVM (arrow), suggesting that the GFP-Rab1A vesicles were internalized into the PV, surrounded by and pinching off from the PVM.

To confirm the morphological feature of the host intra-PV foci, we performed immuno-EM on infected VERO cells expressing GFP-Rab11A using antibodies against GFP. In the PV, we observed multiple membrane-bound structures surrounded by a continuous membrane that were reminiscent of our CLEM images (Fig. 2 D). Gold particles, corresponding to GFP-Rab11A, associated with the membranes of the internal vesicles, suggesting that the host vesicles were encased by another membrane, likely the PVM (Fig. 2 D). Quantification of the vesicle-containing structures present in the PV showed that 18% contained one gold particle, 10% two gold particles, and 72% no gold particles, presumably because these latter vesicles contained other Rab vesicles besides GFP-Rab11A (Fig. 2 E).

Intra-PV host vesicles concentrate in regions containing the IVN

Our fluorescence microscopy analyses illustrate that host GFP-Rab foci were not uniformly dispersed throughout the vacuolar space but tended to concentrate in particular regions, such as in the middle of the PV or in patches near the PVM; this observation was particularly evident for abundantly internalized Rabs (Fig. 3 A). EM observations illustrate that the PV interior is a unique environment containing uncharacterized structures and filaments and is occupied by an IVN of membranous tubules (Sibley et al., 1995). The IVN contains lipids and dense granule proteins secreted by the parasite, including TgGRA2, TgGRA6, TgGRA4, TgGRA8, and TgGRA7. Interestingly, multiple GFP foci were observed in patches of TgGRA7 staining, either on

Downloaded from http://rupress.org/jcb/article-pdf/216/12/4235/1597780/jcb_201701108.pdf by guest on 05 December 2025

the top or edge of the PV, and GFP foci often appeared as beads on a string when viewed in 3D (Fig. 3 A). To further assess whether host intra-PV GFP-Rab vesicles concentrate in regions with the IVN, we immunostained the IVN for other markers, and in each case, we observed a clustering of GFP foci in PV areas densely labeled for the IVN. For example, in single z-slices through the middle of a PV, GFP-Rab11A foci clustered in two distinct regions of the PV: in the middle and in a patch along the edge (Fig. 3 B and Fig. S4, A and B, arrows). These regions also contained TgGRA2, TgGRA4, TgGRA7, or TgGRA8. In some cases, we observed a row of GFP-Rab11A foci that amassed along a stretch of TgGRA protein staining (Fig. 3, B and C; and Fig. S4 B).

We next investigated the association with the IVN in greater detail by EM. At the ultrastructural level, the IVN is composed of intertwined, thin tubules (60–90 nm in diameter; Sibley et al., 1995). Within newly invaded parasites, we observed unique compartments containing long tubules (Fig. 4 A, arrowheads) with a similar morphology to the IVN tubules (Fig. 4 B), likely representing the IVN before secretion by the parasite. Once secreted, the IVN often remains confined to some area of the PV (at the PV center, in patches between parasites, or at one edge of the PV; Fig. 4 B; Sibley et al., 1995). Interestingly, double-membrane vesicles were observed trapped within the IVN (Fig. 4 C, circles) and were reminiscent of host Rab vesicles surrounded by a membrane, as illustrated in our CLEM images. The IVN seems to be a dynamic structure, as some of the IVN tubules appear appended to the PVM (Fig. 4 D, arrows; Sibley et al., 1995; de Souza and Attias, 2015), suggestive of their fusion with the PVM. Interestingly, upon incubation of infected cells with LDL complexed to gold particles to track host endocytic compartments inside the PV, we observed host LDL–containing vesicles, enclosed by a membrane, connected to tubules of the IVN (Fig. 4, E–G, arrowheads), and even in the lumen of individual tubules of the IVN. Examining in serial sections the morphology of an IVN tubule connected to a large membrane-bound structure, we observed that the structure contained multiple individual vesicles, some of which contained LDL-gold particles (Fig. 4 H). Finally, many host LDL–containing vesicles were observed wrapped by the IVN tubules or at least in close proximity to them (Fig. 4, I and J). Jointly, these observations suggest that the IVN tubules connected to the PVM may function as conduits to deliver host organelles into the PV, assigning a potential role of the IVN for the uptake and sequestration of host material into the PV.

The *Toxoplasma* IVN contributes to host vesicle internalization into the PV

We previously documented that the PV is wrapped by host microtubules that further poke into the PVM forming deep invaginations, which may serve as conduits to deliver host endolysosomes into the PV lumen (Coppens et al., 2006). To then examine the contribution of the IVN tubules appended to the PVM to host vesicle internalization into the PV, we monitored the presence of GFP-Rab11A in the PV of parasites with a defective IVN (e.g., *Δgra2Δgra6* or *Δgra2* parasites) or hyperdeveloped IVN (e.g., upon addition of excess oleic acid [OA] to the medium).

TgGRA2 and TgGRA6 are important for the tubulation and maintenance of the IVN, as deletion mutants lack structural IVN (Mercier et al., 2002); *Toxoplasma* lacking *gra2* have decreased infectivity in animals (Mercier et al., 1998; Dou et al., 2014). To assess the role of TgGRA2 and TgGRA6 and, thus, the importance of a functional IVN in host vesicle internalization, we infected cells expressing GFP-Rab11A with *Δgra2Δgra6*, *Δgra2*, *Δgra2::GRA2*, and WT parasites to compare the number and properties of host intra-PV GFP-Rab11A foci (Fig. 5). We did not detect internalized GFP-Rab11A foci in the *Δgra2Δgra6* or *Δgra2* mutants, but we detected multiple GFP-Rab11A foci inside the PV of the WT and complemented strains.

To quantify the internalization defect in mutant parasites defective in the IVN, we created a measurement protocol in Volocity imaging software to measure the number, volume, distance from the PV centroid, and shape factor of intra-PV GFP-Rab11A foci as well as PV shape factor and volume (Fig. S5). Using antibodies to TgGRA7 and TgNTPase, we delineated the PV circumference and identified GFP-Rab11A foci located within the footprint of the PV (Fig. S5). Both *Toxoplasma* mutants had approximately four times fewer intra-PV foci than either WT or *Δgra2::GRA2* parasites (Fig. 5 B). Moreover, the foci were fivefold smaller in these mutants, and their distance from the PV centroid was greater, suggesting that the foci were further from the center and closer to the edge of the PV (Fig. 5, C and D). Both mutants had a slight but statistically significant difference in foci shape factor (Fig. 5 E). The shape of the *Δgra2Δgra6* PV was significantly different from WT and the complemented strain, and the volume of the *Δgra2Δgra6* PV was slightly smaller than the complemented strain (Fig. 5, F and G). The differences in PV shape factor and volume may reflect changes in PV morphology in the absence of the IVN.

To probe the internalization defects in greater detail, we performed EM studies on infected cells incubated with LDL-gold particles to track endocytic structures in the PV (Fig. 6). We first examined the ultrastructure of the IVN in WT parasites compared with *Toxoplasma* lacking *gra2* and/or *gra6* or to parasites incubated with excess OA (Fig. 6 A). In *Δgra2* PVs, we predominantly detected loose whorls of membranes instead of thin tubules organized in a network, as observed in the PV of WT parasites or in the complemented strain (unpublished data). More dramatically, *Δgra2Δgra6* PVs contained solely granular material but no membrane profiles (Fig. 6 A; Mercier et al., 2002; Rommereim et al., 2016). In parasites exposed to excess OA, the structure of the IVN membranes remained unchanged, but the IVN greatly proliferated, occupying the entire vacuolar lumen. For *Δgra2* parasites, we observed host LDL–containing structures in close proximity to and surrounding the PV (Fig. 6 B, arrowheads) and sometimes abutting the PVM (Fig. 6 B, inset). Less than 20% of *Δgra2* PVs harbored host LDL–containing structures, whereas at least one was detected in the majority (∼90%) of WT PVs, 5% of which contained more than four structures (Fig. 6 C and F). Although host LDL–containing structures clustered around the PV of *Δgra2Δgra6* parasites (Fig. 6 D, arrowheads), none were detected in the PV lumen (Fig. 6 F). Our EM analysis confirms that these mutants have a defect in host vesicle internalization. Though the IVN proliferated in OA-treated infected cells, we did not observe any change in the internalization of host LDL–containing endosomes; the majority of PVs contained at least one host LDL structure. Double-mutant parasites *(Δgra2Δgra6*) incubated with excess OA exhibited neither an IVN-like structure nor LDL-containing organelles in the PV (Fig. 6 E). Thus, although the absence of the IVN results in impairment in host vesicle internalization into the PV of mutant parasites, the proliferation of the IVN does not lead to an increased number of host organelles sequestered into the PV.

Downloaded from http://rupress.org/jcb/article-pdf/216/12/4235/1597780/jcb_201701108.pdf by guest on 05 December 2025

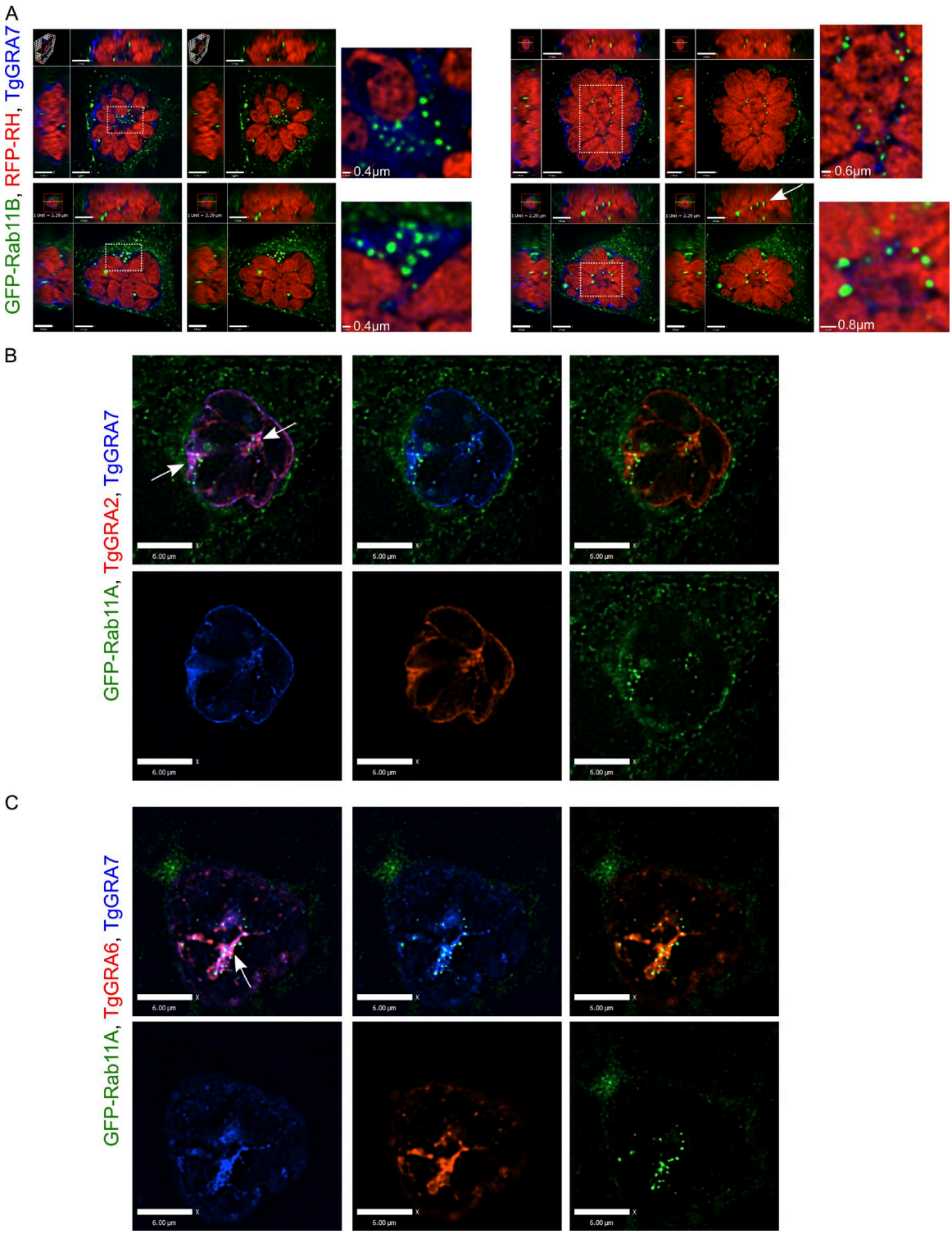

Figure 3. **Localization of host GFP-Rab11A vesicles relative to the IVN.** (A) HeLa cells expressing GFP-Rab11B (green) were infected with RFP-RH for 24 h and immunostained for TgGRA7 (blue). Orthogonal views of the four PVs are shown. An enlargement of the boxed region highlights foci accumulation on the IVN close to the PV periphery (left) or in the middle of the PV. The arrow indicates a row of aligned intravacuolar foci. Bars: (orthogonal views, top, left) 1.7 µm; (top, right) 1.6 µm; (bottom, left and right) 1.8 µm. (B and C) Infected (24 h) VERO cells expressing GFP-Rab11A (green) were immunostained for TgGRA7 (blue) and TgGRA2 (red, B) or TgGRA6 (red, C). Arrows pinpoint patches of IVN where GFP-Rab11A foci are concentrated. Bars: (B and C) 6 µm.

The PVM and IVN-localized protein TgGRA7 induces liposome tubulation and may be involved in the formation of host organelle–sequestering tubulostructures in the PV (Coppens et al., 2006). Δ*gra7* parasites exhibit minor growth delays (Coppens et al., 2006) but have an enlarged IVN. Because host GFP-Rab11A foci concentrate in TgGRA7-containing regions of the IVN, we assessed whether TgGRA7 is involved in GFP-Rab11A internalization. We infected cells

Downloaded from http://rupress.org/jcb/article-pdf/216/12/4235/1597780/jcb_201701108.pdf by guest on 05 December 2025

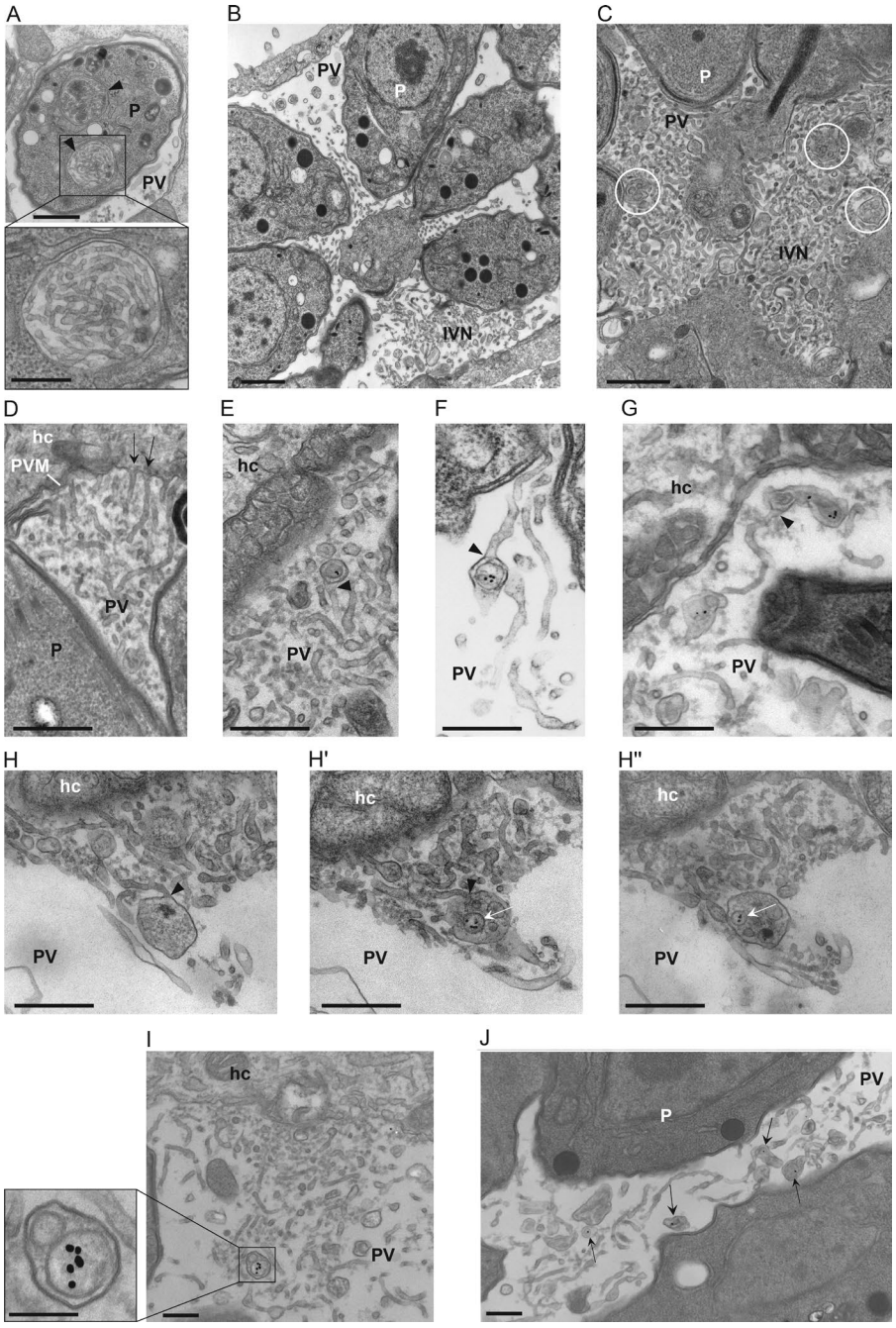

Figure 4. **Localization of host LDL–containing endosomes and the IVN.** (A–D) TEM images of infected VERO cells. (A) Intracellular compartments containing membrane tubules likely of the IVN before secretion (arrowheads). Bars: 200 nm; (inset) 100 nm. (B) Intravacuolar distribution and morphology of the IVN tubules after secretion. Bar, 500 nm. (C) IVN at the center of a PV with membrane-bound structures containing vesicles likely originating from the host cell (white circles). Bar, 150 nm. (D) Connection of IVN tubules with the PVM (arrows). Bar, 200 nm. (E–J) TEM images of infected VERO cells incubated with LDL-gold for 24 h. (E–G) Detection of intra-PV host LDL-containing endocytic structures within a tubule of the IVN (arrowheads). Bars, 200 nm. (H–H″) Shown are serial sections of an intra-PV, membrane-bound structure that is attached to an IVN tubule and contains several host LDL–containing vesicles (arrows). Bars, 150 nm. (I and J). Membrane-bound structures, unattached to IVN tubules, with host LDL vesicles (arrows) in regions enriched in the IVN. Bars, 200 nm. hc, host cell; P, parasite.

Downloaded from http://rupress.org/jcb/article-pdf/216/12/4235/1597780/jcb_201701108.pdf by guest on 05 December 2025

expressing GFP-Rab11A with *Δgra7* and WT parasites to compare the number and properties of intra-PV host foci. No statistically significant differences were observed in the number, volume, or distance to the PV centroid of GFP-Rab11A foci in PVs of *Δgra7* and WT parasites with comparable vacuole size (Fig. S4, C–H).

A phospholipase localizes to the IVN membranes surrounding host Rab vesicles

Among the dense granule proteins secreted by *Toxoplasma* into the PV is a lecithin:cholesterol acyltransferase, TgLCAT. TgLCAT catalyzes the release of fatty acids from phospholipid membranes, resulting in the production of lysophospholipids, which destabilize membranes (Pszenny et al., 2016). LCAT-deficient *Toxoplasma* are impaired in their development in vitro and infectivity in animals, whereas parasites overexpressing TgLCAT are more infectious than WT (Pszenny et al., 2016). The function and substrates of TgLCAT inside the PV, however, are still unknown. As a first step in analyzing the role of TgLCAT in the PV, we examined the distribution of TgLCAT in the PV by IFA using antibodies against various PV markers (Fig. 7 A and Fig. S4). As previously described, we detected TgLCAT in dense granules within the parasites and in patches in the vacuolar space. Within the PV, TgLCAT staining was concentrated in the center and along the interior edge of the PVM, but not on the PVM (Fig. 7 A, arrows). TgLCAT colocalized with the IVN proteins TgGRA3, TgGRA4, TgGRA6, and TgGRA7 (Fig. 5 A and Fig. S4, G and H). In fact, the MOC for TgGRA4 and TgGRA7 in relation to TgLCAT was 0.92 and 0.754, respectively. We confirmed the localization

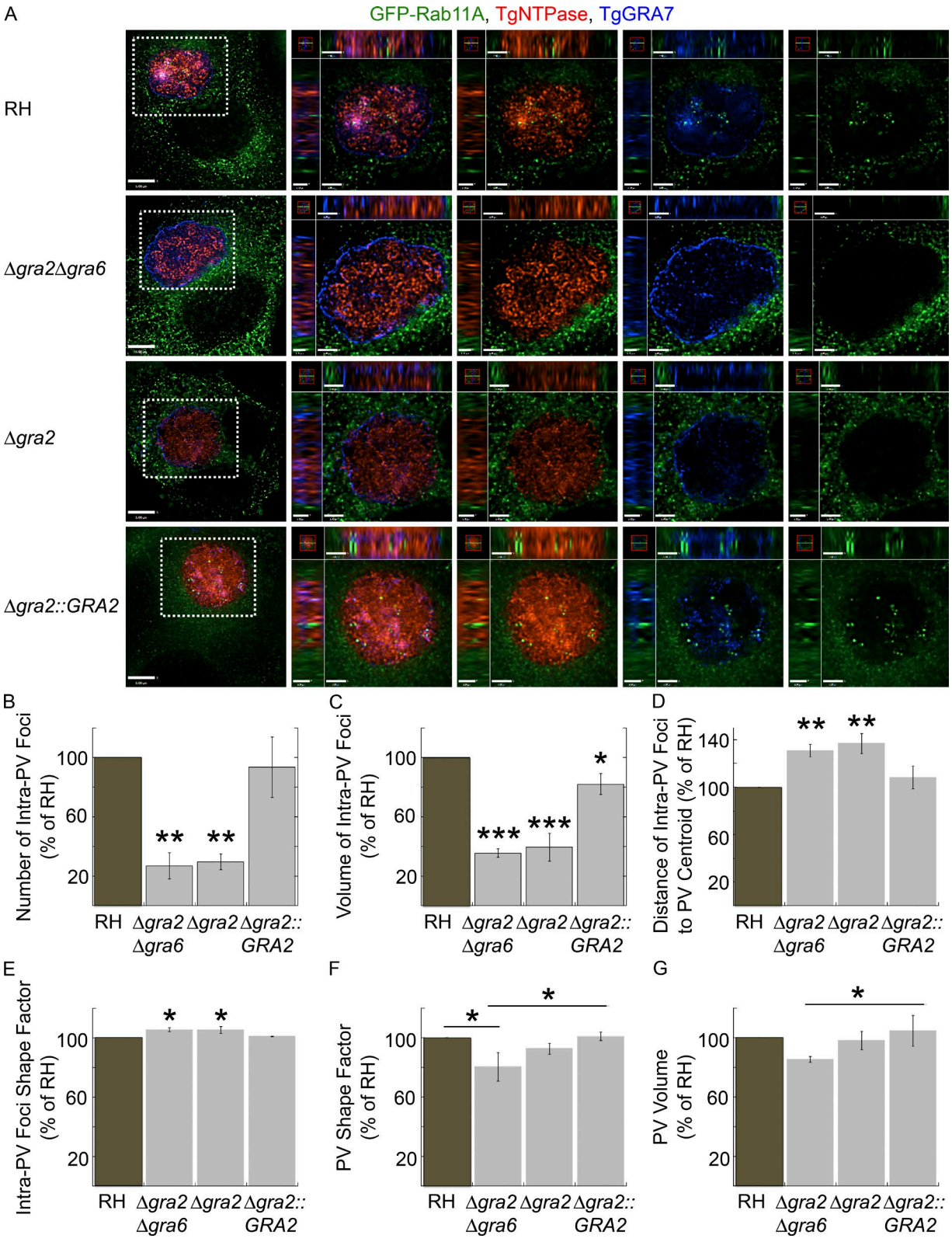

Figure 5. **Role of TgGRA2 and TgGRA6 on the internalization of host GFP-Rab11A into the PV.** (A–D) VERO cells expressing GFP-Rab11A (green) were infected with RH, *Δgra2Δgra6*, *Δgra2*, and *Δgra2::GRA2* parasites for 24 h and then fixed and immunostained for TgNTPase (red) and TgGRA7 (blue). (A) Individual z-slices are shown with the boxed region magnified in the orthogonal views, highlighting the PV. Bars: 6 µm; (orthogonal views for RH and *Δgra2Δgra6*) 1.3 µm; (orthogonal views for *Δgra2* and *Δgra2::GRA2*) 1.4 µm. (B–G) The number (B), volume (C), distance from the PV centroid (D), and shape factor (E) of intravacuolar GFP-Rab11A foci with the shape factor (F) and volume (G) of PVs calculated for PVs containing 16 parasites. Mean values ± SD, *n* = 3 independent experiments. PVs measured: RH (23–25), *Δgra2Δgra6* (19–22), *Δgra2* (19–21), and *Δgra2::GRA2* (23–26). *, P < 0.03; **, P < 0.001; ***, P < 0.0001.

Downloaded from http://rupress.org/jcb/article-pdf/216/12/4235/1597780/jcb_201701108.pdf by guest on 05 December 2025

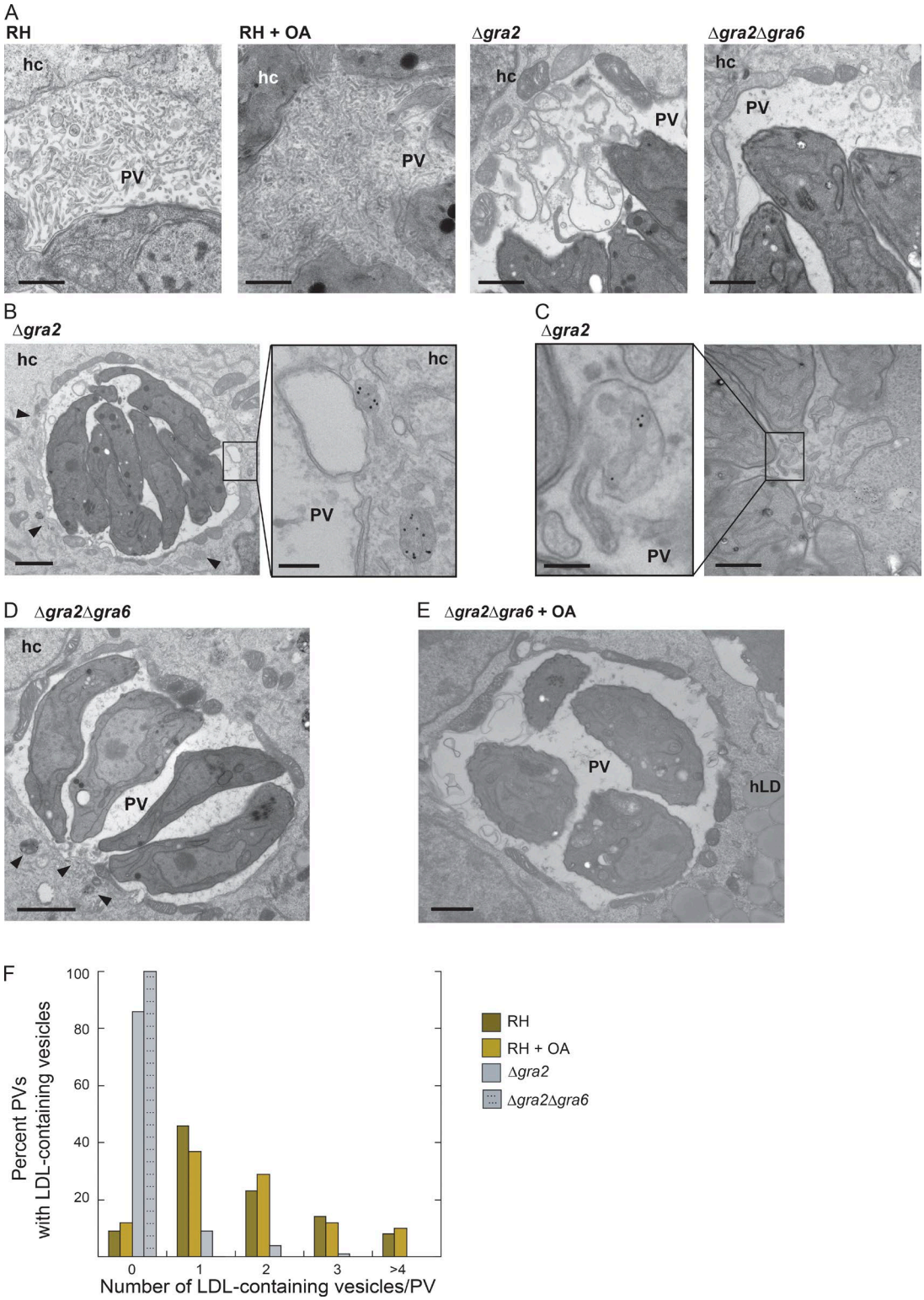

Figure 6. **Role of TgGRA2 and TgGRA6 on the internalization of host LDL-containing endosomes into the PV.** (A) TEM of PVs in HFF (24 h): RH, RH with exogenously added 0.2 mM OA, *Δgra2*, and *Δgra2Δgra6* parasites. Bars, 400 nm. (B and C) *Δgra2* infected VERO cells (24 h) incubated with LDL-gold complexes for 20 h. (B) *Δgra2* PV with host LDL–containing endosomes (arrowheads) along the edge of the PV in the host cytosol. Bars: 800 nm; (inset) 200 nm. (C) Example of a few *Δgra2* PVs with intra-PV host LDL–containing endosomes. Bars: 300 nm; (inset) 200 nm. (D) *Δgra2Δgra6*-infected VERO cells (24 h) incubated with LDL-gold for 20 h. Arrowheads indicate LDL-containing endosomes outside the PV. Bar, 800 nm. (E) *Δgra2Δgra6* infected VERO cells with exogenously added 0.2 mM OA. Bar, 800 nm. (F) The percentage of PVs with different abundances of intra-PV host LDL–containing endosomes.

Downloaded from http://rupress.org/jcb/article-pdf/216/12/4235/1597780/jcb_201701108.pdf by guest on 05 December 2025

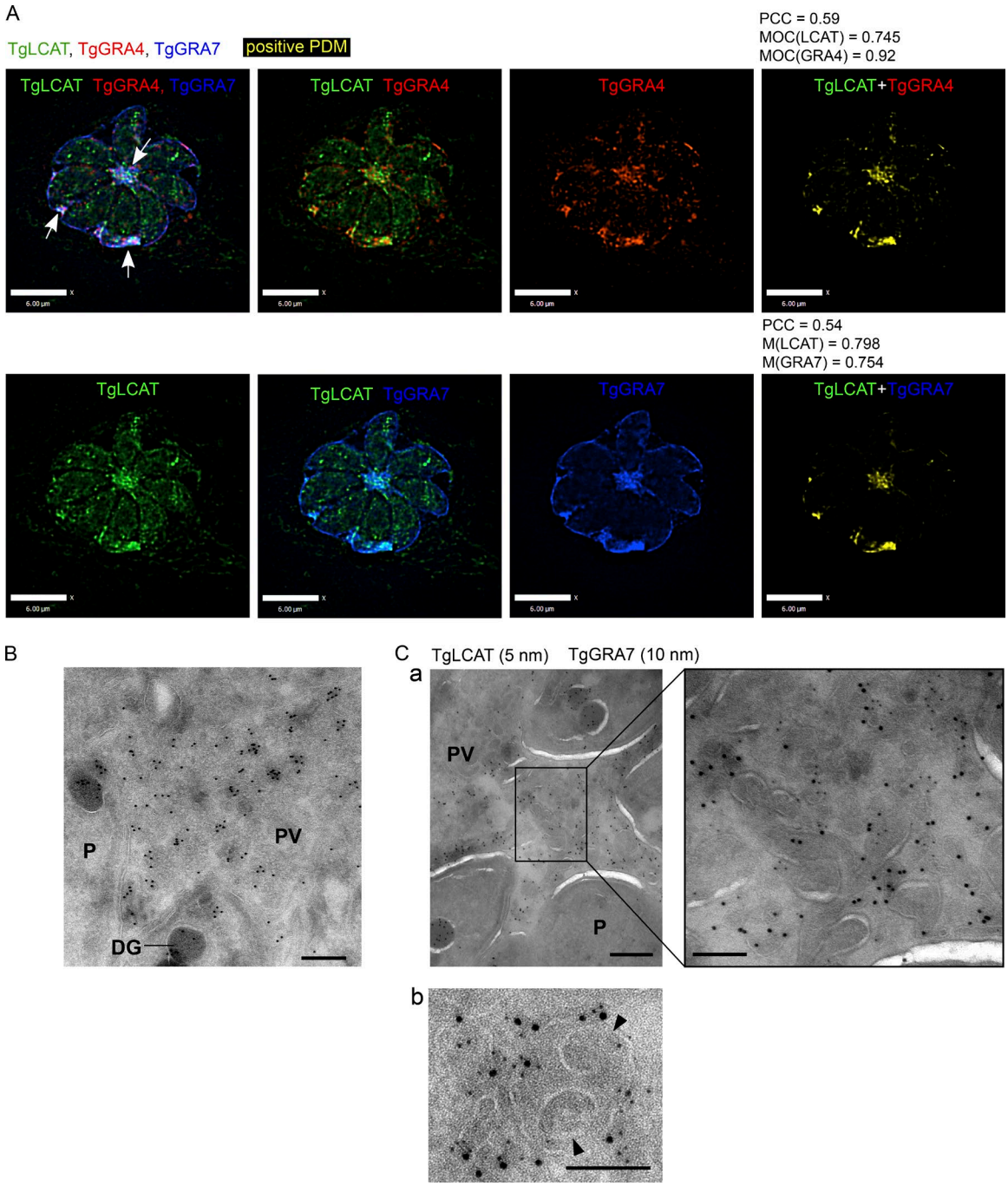

Figure 7. **Localization of the *Toxoplasma* lipolytic lecithin/cholesterol acyltransferase (TgLCAT) to the IVN.** (A) Infected HFF cells (24 h) were immunostained for TgLCAT (green), TgGRA4 (red), and TgGRA7 (blue), and a positive product of the difference of the mean (PDM) image (yellow), PCC, and MOC were calculated. Arrows indicate TgLCAT colocalized with the IVN. Bars, 6 µm. (B and C) Immuno-EM of HFF cells infected with Δ*lcat*:LCAT-HA with anti-HA for 24 h showing TgLCAT on the IVN colocalized with TgGRA7 (a) and on double membrane structures (b). Arrowheads in b point to internal vesicles likely from the host cell surrounded by the PVM. Bars: 200 nm; (a, inset) 100 nm.

of TgLCAT on the IVN by immuno-EM (Fig. 7, B and C). We observed both TgLCAT and TgGRA7 present on the tubules of the IVN (Fig. 7 C, panel a, inset) and on the outer membrane of double-membrane vesicles (Fig. 7 C, panel b). Neither TgLCAT nor TgGRA7 localized to the membranes of the inner vesicles, likely corresponding to host vesicles (Fig. 7 C, panel b).

Because TgLCAT activity can lead to the destabilization of membranes (Pszenny et al., 2016), an intriguing hypothesis is that TgLCAT may degrade the limiting membrane of PV-localized host Rab vesicles, promoting the release of their cargo into the PV. To determine the localization of TgLCAT in relation to host Rab vesicles, we infected cells expressing GFP-Rab11A with TgLCAT-HA–tagged parasites and processed the samples for IFA (Fig. 8 A). GFP-Rab11A foci were concentrated in the center of the PV, in a region enriched in TgLCAT and TgGRA7 and, by extension, the IVN. In the central patch, the TgLCAT staining had a honeycomb-like structure, whereas the TgGRA7 staining was more evenly distributed. Interestingly,

Downloaded from http://rupress.org/jcb/article-pdf/216/12/4235/1597780/jcb_201701108.pdf by guest on 05 December 2025

the GFP-Rab11A foci localized primarily within and between the holes in the TgLCAT staining pattern (Fig. 8 A). The GFP-Rab11A foci were also found in the middle of a cavity surrounded by TgGRA7 and, at times, colocalized with TgGRA7 (Fig. 8 A, circles), which may represent Rab11A foci on the PVM. To analyze the localization in finer detail, we inspected infected cells expressing GFP-Rab11A by immuno-EM. TgLCAT was distributed throughout membranous structures in the PV, both between parasites (Fig. 8 B) and near the parasite's basal end (Fig. 8 C). TgLCAT localized along both tubular and rounded structures within the PV (Fig. 8 B). GFP-Rab11A was observed on the membranes of vesicles within the PV, although it was found on fewer structures than TgLCAT (Fig. 8 B). GFP-Rab11A predominantly localized to the inner membrane of the double membrane vesicles, whereas TgLCAT was often observed on membranes encircling the GFP-Rab11A containing vesicles (Fig. 8 C).

Parasites overexpressing TgLCAT contain fewer Rab vesicles in the PV

To analyze the potential role of TgLCAT in processing host vesicles inside the PV via its phospholipase activity, we measured the number, volume, and distance to the PV centroid of intra-PV host GFP-Rab11A vesicles for parasites deleted for and overexpressing TgLCAT (Fig. 8, D–G). Compared with parental parasites, *Δlcat::LCAT-HA* expresses approximately three times more TgLCAT protein (Pszenny et al., 2016). The strain overexpressing TgLCAT had fewer intra-PV foci than either WT or *Δlcat* parasites (Fig. 8 D). There was no statistically significant difference in the volume of the intra-PV Rab11A foci for any of the strains (Fig. 8 E). However, the intra-PV foci of the strain overexpressing TgLCAT were closer to the PV centroid than for either WT or *Δlcat* (Fig. 8 F). The PVs of *Δlcat::LCAT-HA* parasites were statistically smaller than those of the other strains (Fig. 8 G). Thus, deleting TgLCAT had no effect on the abundance or localization of intra-PV host GFP-Rab11A vesicles whereas overexpressing TgLCAT led to fewer intra-PV foci that were closer to the PV centroid and smaller PVs. This suggests that increased activities of TgLCAT in the PV impact the fate of intravacuolar host Rab vesicles, possibly by promoting their degradation to liberate their content for the parasite.

GFP-Rab11A accumulates in a few *Δcpl* parasites

Toxoplasma can internalize host cytosol–derived GFP in a process requiring the cathepsin protease L that resides in VAC, a parasite endosomal compartment (Parussini et al., 2010; Dou et al., 2013) To determine whether host Rab released from intra-PV foci could also be taken up by the parasite, we infected GFP-Rab11A-expressing CHO or VERO cells with *Δcpl* parasites to slow down potential degradation of GFP-Rab11A in VAC. In a small number of *Δcpl* parasites, we observed one large intraparasitic punctate fluorescent signal, suggesting that *Toxoplasma* also accesses host material originating from Rab vesicles (Fig. 8 H).

Δgra2Δgra6 parasites display abnormal membrane properties

Previously, we showed that expressing dominant negative host Rab14 and Rab43 resulted in a reduction in host-derived sphingolipids in the PV (Romano et al., 2013), suggesting a role for host Rabs in delivering lipids to the parasite. Because Rab vesicles accumulate within the IVN, we addressed whether lipid scavenging is impacted by the absence of an IVN in *Δgra2Δgra6* PVs. Cells infected with mutant or WT parasites were incubated with BODIPY TR ceramide for 5 or 40 min (Fig. 9, A and B). No difference in fluorescence intensity was observed between the two PV populations after a 5-min pulse of BODIPY TR ceramide. However, significant differences were noticed in the distribution of the fluorescent signal, with the majority of WT PVs exhibiting a stronger staining of the PVM and in large intra-PV patches, whereas most of the mutant displayed stronger signal at the plasma membrane and organelles (Fig. 9 A). Both PVs displayed a strand-like fluorescent signal that often extended from the PVM into the PV (Fig. 9 A, arrows). After a 40-min pulse, both strains were similarly stained (Fig. 9 B).

Differences in the initial distribution of host sphingolipids in the *Δgra2Δgra6* PV was not the only membrane disparity observed. One unique property of the PVM is its ability to form projections (PVM projections [PVMPs]) decorated with parasite proteins (e.g., TgGRA3, TgGRA7, and TgGRA14) into the host cytosol, and some PVMPs interact with host organelles (Dubremetz et al., 1993; Jacobs et al., 1998; Rome et al., 2008; Romano et al., 2013). By immunostaining the PVM with anti–GRA7 antibodies 20 h after tinfection, we observed a greater percentage of Δ*gra2*Δ*gra6* PVs displaying PVMPs often forming an intricate web-like pattern in the host cytoplasm (Fig. 9 C). Thus, deleting TgGRA2 and TgGRA6 significantly alters parasite membrane properties.

Discussion

As master regulators of cellular homeostasis, Rab GTPases are often prime targets of intracellular pathogens that exploit the function of specific Rab proteins in a way that benefits their intracellular lifestyle. In this study, we used GFP-tagged Rab proteins as markers of different trafficking pathways to identify which pathways are targeted by *Toxoplasma* and as a means of identifying parasite proteins involved in host Rab vesicle internalization and processing in the PV. Our data demonstrate that the parasite diverts a broad range of host Rab vesicles, though with some selectivity, as host Rabs involved in anterograde, recycling, and endocytic pathways are preferentially targeted by *Toxoplasma*.

Interception of host Rab trafficking pathways by *Toxoplasma* may be involved in different aspects of the parasite's program of infectivity: dysregulation of host trafficking pathways, immune modulation, and/or nutrient scavenging (Fig. 9 D). The fact that the Rab1 tethering factor p115 is not internalized into the PV along with Rab1 may suggest a dysregulation of ER–Golgi trafficking via interference with the interaction of Rab1 and its effectors, possibly by an as-yet-undiscovered parasite effector. Alternatively, the parasite may internalize a subpopulation of Rab1 membranes that do not contain p115. As a case in point, Rab1 and p115 display variable overlap in the pericentrosomal intermediate compartment, suggesting the presence of different subdomains (Saraste, 2016). As the centrosome is relocated to the PV during infection, the pericentrosomal intermediate compartment would be close to the PV and may represent a source of Rab1 membranes devoid of p115. The interception of host Rab1 vesicles, together with Golgi-derived Rabs, may also be the cause of host Golgi fragmentation into ministacks observed during a *Toxoplasma* infection (Romano et al., 2013), as Rab1 dominant-negative mutants lead to Golgi

Downloaded from http://rupress.org/jcb/article-pdf/216/12/4235/1597780/jcb_201701108.pdf by guest on 05 December 2025

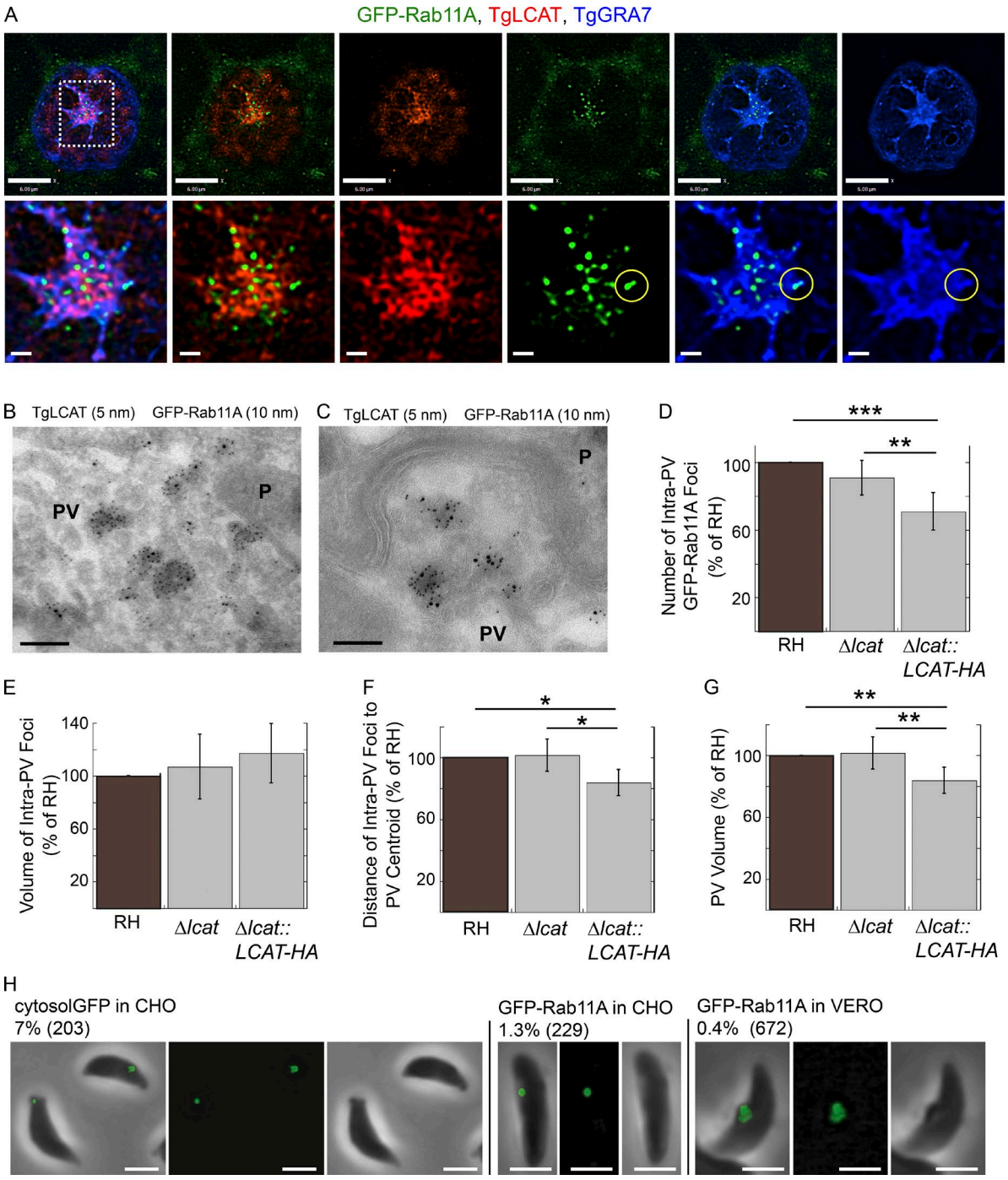

Figure 8. **Distribution of TgLCAT relative to intra-PV host GFP-Rab11A vesicles.** (A) GFP-Rab11A–expressing VERO cells (green) infected with *Δlcat::LCAT-HA* (24 h) were immunostained for HA (red) and TgGRA7 (blue). The yellow circle indicates an overlap of GFP-Rab11A and TgGRA7. Bars: 6 µm; (magnified views) 0.4 µm. (B and C) Double immuno-EM for GFP and HA of VERO cells expressing GFP-Rab11A and infected with *Δlcat::LCAT-HA* (24 h) showing codistribution. Bars, 100 nm. (D–G) GFP-Rab11A–expressing VERO cells infected with RH, *Δlcat,* and *Δlcat::LCAT-HA* parasites (24 h). The number (D), volume (E), and distance from the PV centroid (F) of intravacuolar GFP-Rab11A foci and the volume (G) of the PV were calculated. The data represent mean values ± SD, *n* = 6 independent experiments. Number of PVs measured: RH (24, 17, 8, 38, 38, and 35), *Δlcat* (14, 22, 10, 40, 41, and 31), and *Δlcat::LCAT-HA* (18, 16 7, 34, 33, and 38) *, P < 0.05; **, P < 0.01; ***, P < 0.0002. (H) CHO cells transiently expressing GFP (cytosol GFP) or GFP-Rab11A (24 h) or VERO cells stably expressing GFP-Rab11A were infected with *Δcpl* parasites for 24 h. Parasites were mechanically liberated from host cells and viewed by fluorescence microscopy. Shown are overlay, fluorescence, and phase contrast images. The percentage of parasites positive for staining is shown along with the number of parasites viewed. Bars, 2 µm.

fragmentation (Wilson et al., 1994). Interception of host Rab pathways may also affect immune modulation, as Rab22A is recruited to the PV for the control of MHC-I intracellular trafficking (Cebrian et al., 2016). Lastly, the interception of host Rab pathways may be used by the parasite for nutrient scavenging. For example, *Toxoplasma* scavenges sphingolipids from host Golgi–derived Rab GTPases (Rab14, Rab30, and Rab43) into the PV, and expression of dominant-negative Rab14 and

Downloaded from http://rupress.org/jcb/article-pdf/216/12/4235/1597780/jcb_201701108.pdf by guest on 05 December 2025

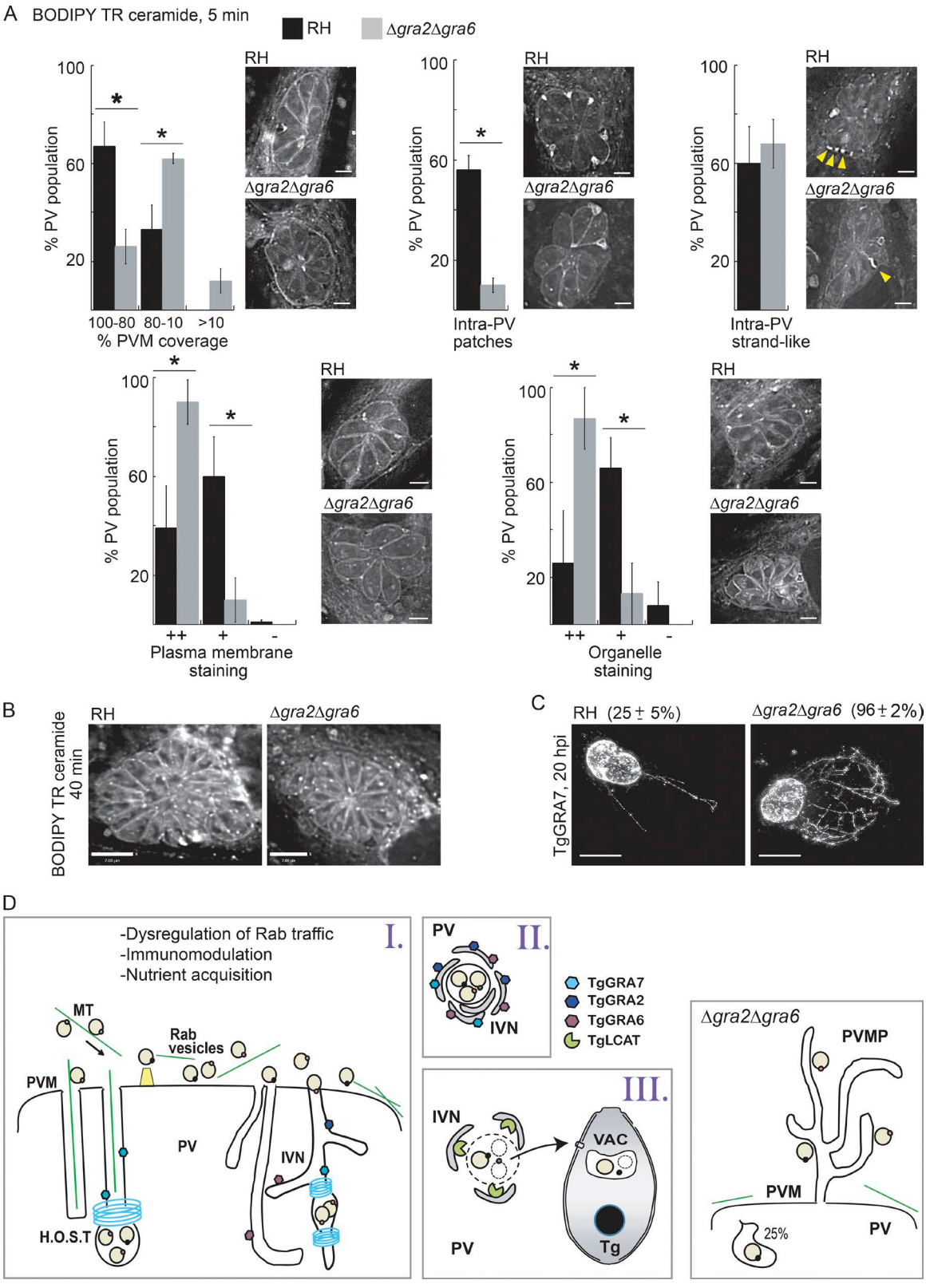

Figure 9. **Distribution of host derived ceramides in the PV and parasites.** (A and B) HFF cells infected with RH or *Δgra2Δgra6* parasites (20 h) were incubated with BODIPY TR C5-ceramide for 5 min (A; bars, 3 µm) or 40 min (B; bars, 7 µm) and fixed and viewed by fluorescence microscopy. Individual z-slices are shown. For the 5-min treatment, PVs containing eight parasites were placed into categories based on their staining pattern as described in Materials and methods. Arrowheads in A show filamentous structures connecting the PVM with parasites. *, $P < 0.005$. (C) HeLa cells were infected with RH or *Δgra2Δgra6* parasites (20 h) and immunostained for TgGRA7 to detect PVM projections (PVMPs). Total intensity projections of z-stacks and percentage of the PV population with PVMPs (mean ± SD) are shown. *, $P < 0.0001$. Bars, 7 µm. (D) Hypothetical model of host vesicles internalized into the PV in WT (left cartoons) and *Δgra2Δgra6* parasites. H.O.S.T., host organelle–sequestering tubulostructures.

Downloaded from http://rupress.org/jcb/article-pdf/216/12/4235/1597780/jcb_201701108.pdf by guest on 05 December 2025

Rab43 results in a reduction of host-derived sphingolipids in the PV (Romano et al., 2013).

Our model for the internalization and processing of host vesicles in the PV involves the following steps: (1) transport to the PV, internalization via tubules, and detachment from the PVM; (2) encircling by IVN tubules; and (3) enzymatic destabilization of membranes and uptake of cargo by the parasite (Fig. 9 D).

First, host vesicles are directionally transported to the PV along microtubules as host microtubules encase the PV, and treatment of infected cells with Taxol interrupts the trafficking of endolysosomes toward the PV (Coppens et al., 2006; Walker et al., 2008), suggesting a manipulation of microtubule-mediated vesicle trafficking by the parasite. It is therefore conceivable that host Rab vesicles are also dispatched to the PV along microtubules. A recognition event of host Rab vesicles mediated by parasite proteins at the PVM potentially would the potentially occur, allowing discrimination between host membranes. The next step involves the penetration of host Rab vesicles into the PV via invaginations of the vacuolar membrane. We detected endocytic organelles (containing LDL absorbed onto gold particles) in two different tubular structures in the PV: (1) in tubules containing a host microtubule derived from the invaginations of the PVM mediated by host microtubules, and (2) in the tubules of the IVN (Coppens et al., 2006). Both structures are attached to the PVM, forming a conduit for the internalization of host material (e.g., proteins and small organelles). These two tubular structures are often seen on the same PV section, suggesting two paths developed by the parasite to divert host structures. Besides their different origin, the host microtubule–containing tubules are straighter and larger than the IVN tubules, which appear more convoluted. Interestingly, we also observed hybrid tubular structures that contain host microtubules and are connected to IVN tubules, suggesting dynamic fusion events. Next, the tubules containing host vesicles detach from the PVM and relocalize to regions populated with IVN tubules in the PV lumen. Both microtubule-containing and IVN tubules contain GRA proteins and are often covered by an electron-dense coat that constricts their diameter and resembles the dynamin coat at the neck of mammalian clathrin-coated pits (Coppens et al., 2006). If the protein coat is further involved in membrane scission, it could then induce the detachment of Rab vesicles from the PVM and entrap them in the PV lumen.

Second, the released membrane-bound compartment containing clusters of host vesicles are densely wrapped by many IVN tubules decorated with resident proteins. We also observed a similar phenomenon with host lipid droplets internalized into the PV (Nolan et al., 2017).

Third, membranes surrounding the clusters of host vesicles are destabilized by the actions of an IVN localized phospholipase, TgLCAT. Host Rab vesicles are encircled by TgLCAT-containing tubules, and fewer host Rab foci are observed in the PV of a TgLCAT-overexpressor strain, suggesting increased lipolytic activities toward host Rab vesicles and dispersion of host vesicles in the PV lumen. The concept of the IVN serving as a platform for the degradation of host structures mediated by TgLCAT is further supported by our recent data showing that TgLCAT-deficient parasites contain fewer lipids originating from host lipid droplets than WT parasites (Nolan et al., 2017). Material liberated from the host vesicles may become available for the parasite. *Toxoplasma* is able to take up host cytosolic proteins (e.g., GFP) that transverse the PV and digest them in a cathepsin L–dependent manner inside a parasite acidified organelle named VAC; in *Δcpl* mutants, GFP is detected in the VAC compartment (Dou et al., 2014). When mammalian cells expressing GFP-Rab11A were infected with *Δcpl* parasites, we detected a GFP-positive punctate compartment in a small percentage of parasites, suggesting that the parasite may be able to internalize host proteins liberated from intra-PV vesicles.

Lastly, the Δ*gra2*Δ*gra6* mutant that is defective in IVN tubules (Mercier et al., 2002) shows a reduction in the internalization of host vesicles into the PV. Despite ∼75% fewer Rab vesicles trapped in the PV, Δ*gra2*Δ*gra6 Toxoplasma* can salvage host ceramides and has no obvious replication delay in cultured cells, although the absence of TgGRA2 partially attenuates the virulence of *Toxoplasma* during the acute phase of infection (Mercier et al., 1998). If the diversion of Rab vesicles is related to nutrient acquisition, this suggests that the limited number of intra-PV Rab vesicles may provide sufficient lipids for the mutant parasites. Alternatively, the mutant may have developed compensatory mechanisms to acquire nutrients, such as the recruitment of the host ceramide transfer protein CERT for ceramide uptake, as established for *Chlamydia trachomatis* (Derré et al., 2011). As additional pathways, we observed "strands" of BODIPY TR ceramide staining that appeared to connect to the PVM in the PVs of WT and mutant parasites. If these structures transit host sphingolipids into the PV, the mutant may rely solely on this pathway, which may explain the differential distribution of host sphingolipids between WT and mutant PVs. In addition, Δ*gra2*Δ*gra6 Toxoplasma* forms an enlarged network of PVMPs. Our previous study illustrates that some PVMPs form physical contact with host organelles (Romano et al., 2013). Thus, the Δ*gra2*Δ*gra6 Toxoplasma* may use PVMPs to advantageously sort and attract nutrient-filled organelles to the PV, mirroring the IVN function inside the PV of WT parasites.

Materials and methods

Reagents, antibodies, and plasmids

All reagents were obtained from Sigma-Aldrich, unless otherwise stated. BODIPY TR C5-ceramide complexed to BSA was obtained from Thermo Fisher Scientific. The following primary antibodies were used in this study: rat monoclonal and rabbit polyclonal anti-GRA7 (Coppens et al., 2006) and mouse monoclonal anti-GRA2, rabbit polyclonal anti-GRA4, rabbit polyclonal anti-GRA6, and mouse monoclonal anti-GRA8 (provided by J.-F. Dubremetz, Université of Montpellier, Montpellier, France). Commercial antibodies include rabbit monoclonal anti-Rab11 (D4F5; Cell Signaling Technologies), rabbit anti-GFP polyclonal antibodies (A6455; Thermo Fisher Scientific), mouse monoclonal anti-HA.11 (16B12; BioLegend), mouse monoclonal anti–lysobisphosphatidic acid (6C4; Echelon Biosciences Inc.), and mouse monoclonal anti-LIMP/LAMP3/CD63 (H5C6; Developmental Studies Hybridoma Bank; Young and Black, 2004; Bampton et al., 2005). Secondary antibodies used were: goat anti-rat, anti-rabbit, and anti-mouse conjugated to Alexa Fluor 488, 594, or 350 (Thermo Fisher Scientific). OA–BSA complexes were prepared as described previously (Nolan et al., 2017) by dissolving sodium oleate in water at a concentration of 100 mM, followed by vortexing for 3 min with 5% fatty acid–free BSA to reach a final concentration of 10 mM OA–BSA complexes. LDLs adsorbed to 15-nm gold particles were prepared as described previously (Coppens et al., 1987). The plasmids used in this study include pmaxGFP (Lonza), GFP-Rab1A, GFP-Rab1A Q70L,

Downloaded from http://rupress.org/jcb/article-pdf/216/12/4235/1597780/jcb_201701108.pdf by guest on 05 December 2025

GFP-Rab1A S25N, GFP-Rab5A, GFP-Rab7A, and GFP-p115 plasmids provided by C. Roy (Yale University School of Medicine, New Haven, CT; Kagan and Roy, 2002; Kagan et al., 2004); GFP-Rab2A, GFP-Rab14, GFP-Rab24, GFP-Rab30, and GFP-Rab43 plasmids provided by J. Presley (McGill University, Montreal, Canada; Dejgaard et al., 2008); GFP-Rab4A, GFP-Rab6A, GFP-Rab10, GFP-Rab11A, and GFP-Rab11B plasmids provided by M. Scidmore (Cornell University College of Veterinary Medicine, Ithaca, NY; Rzomp et al., 2003); GFP-Rab9A plasmid provided by S. Pfeffer (Stanford University, Stanford, CA; Barbero et al., 2002); and GFP-HRas, GFP-NRas, GFP-KRas4A, and GFP-KRas4B provided by M. Philips (New York University School of Medicine, New York, NY).

Cell culture and transfection

VERO cells, HeLa cells, CHO cells, and human foreskin fibroblasts (HFF) were purchased from the American Type Culture Collection. All cells were maintained at 37°C in a 5% CO_2 atmosphere and grown in either Alpha MEM (with Earle's salts without ribonucleosides, deoxyribonucleosides, and glutamine) or DMEM (with 4.5 g/l glucose and sodium pyruvate without L-glutamine; Corning Cellgro). Unless otherwise stated, media was supplemented with 10% (vol/vol) FBS, 2 mM L-glutamine (Corning Cellgro), and 100 U/ml penicillin plus 100 mg/ml streptomycin (Quality Biological). HeLa cells were transiently transfected using 2 µg plasmid DNA and the Amaxa Nucleofector solution R according to the manufacturer's instructions using program I-013 (Lonza) or with 0.25 µg plasmid DNA and JetPrime reagent according to the manufacturer's instructions (Polyplus-transfection SA). To engineer a stable cell line expressing GFP-Rab11A, the GFP-Rab11A plasmid was linearized with *Apa*L1 and transfected into VERO cells using 2 µg of linearized plasmid, the Amaxa Nucleofector solution R, and program V-01, according to the manufacturer's instructions. Stable clones were selected with 800 µg/ml G418 sulfate (Corning Cellgro) in Alpha MEM with 20 mM Hepes and cloned in serial dilutions in 96-well plates.

Parasite strains and infection conditions

The tachyzoite RH strain (type I lineage) of *Toxoplasma* was used in this study. The RH strain stably expressing RFP was generously provided by F. Dzierszinski (McGill University, Montreal, Canada; Dzierszinski et al., 2004), RH deleted for *gra2* (*Δgra2*) and the corresponding complemented strain (*Δgra2::GRA2*) were provided by V. Carruthers (University of Michigan, Ann Arbor, MI; Mercier et al., 1998, 2002; Dou et al., 2014), RH deleted for both *gra2* and *gra6* (*Δgra2Δgra6*) was generously provided by M.-F. Cesbron-Delauw (Université Grenoble Alpes, Grenoble, France; Mercier et al., 2002). The RH strain deleted for *cpl* (*Δcpl*) was generously provided by V. Carruthers (Larson et al., 2009). The RH strain deleted for *lcat (Δlcat)* and its complement with *LCAT-HA* (*Δlcat::LCAT-HA*) and the RH strain deleted for *gra7 (Δgra7*) were described previously (Coppens et al., 2006; Pszenny et al., 2016). The tachyzoite Nc-Liv isolate of *N. caninum* was used in this study (Barber et al., 1993). All parasites were propagated in vitro by serial passage in monolayers of HFF (Roos et al., 1994). Unless otherwise stated, HeLa cells, VERO cells and VERO cells stably expressing GFP-Rab11a were grown to ∼65% confluence and HFF to confluence before infection with *Toxoplasma* parasites for 30 min at 37°C and 5% CO_2, washed with phosphate-buffered saline (PBS) to remove extracellular parasites, and incubated at 37° and 5% CO_2 at the indicated times. To track host endocytic organelles, LDL complexed to colloidal gold was added exogenously to infected cells. First, VERO cells were grown in Alpha MEM medium and incubated at 37°C in 5% CO_2 for 24–48 h. Second, the medium was replaced with Alpha MEM supplemented with 10% (vol/vol) delipidated FBS (Cocalico Biologicals) and the cells were incubated at 37°C in 5% CO_2 for 20 h. Third, the cells were infected with *Toxoplasma* parasites (RH, *Δgra2*, or *Δgra2Δgra6*) for 3.5 h in Alpha MEM and incubated at 37°C in 5% CO_2. Fourth, cells were washed with PBS to remove extracellular parasites, which was confirmed by light microscopy. Last, infected cells were incubated with LDL-gold particles with or without 0.2 mM OA in Alpha MEM for 18 h and processed for EM.

Cell labeling

Infected cells were incubated in serum-free medium containing 5 µM BODIPY TR C5-ceramide conjugated to BSA for 5 or 40 min, washed with PBS and fixed with 4% paraformaldehyde (Electron Microscopy Sciences) for 15 min, washed with PBS, rinsed with water and mounted on slides using ProLong Diamond antifade mounting solution (Thermo Fisher Scientific).

For the GFP-Rab11A parasite acquisition assay, CHO cells transiently transfected for 24 h with maxGFP or GFP-Rab11A or VERO cells stably expressing GFP-Rab11A were infected with RH*Δcpl* parasites for 24 h. Parasites were mechanically liberated from host cells by syringe lysis and filter (3 µm) purified. Parasites were pelleted, washed with cold PBS, and fixed with 4% formaldehyde (Polysciences) and 0.02% glutaraldehyde (EMS) for 15 min. Fixed parasites were washed with PBS and mounted with ProLong Diamond mounting solution on 0.01% polylysine–coated slides.

For immunolabeling, cells were fixed in PBS with 0.02% glutaraldehyde (EM grade; EMS) and either 4% formaldehyde (Polysciences, Inc.) or 4% paraformaldehyde (Electron Microscopy Sciences) for 15 min and permeabilized with 0.3% Triton X-100 in PBS for 5 min. Cells were incubated in blocking buffer (3% BSA, Fraction V; Thermo Fisher Scientific; in PBS) for 1 h followed by incubation in primary antibody diluted in blocking buffer for 1 h to overnight. Cells were washed three times with PBS for 5 min each and then incubated in secondary antibody diluted in blocking buffer for 1 h and washed three times with PBS for 5 min each. In some cases, cells were incubated in a 1:1,000 dilution of 1 mg/ml DAPI (Roche Diagnostics) in PBS for 5 min followed by three washes with PBS. Coverslips were rinsed with water and mounted on slides with ProLong antifade mounting solution (Alexa secondary antibodies) or ProLong Diamond antifade mounting solution (GFP or RFP).

Fluorescence microscopy

Fixed samples were viewed with either a Nikon Eclipse 90i fluorescence microscope equipped with an oil-immersion Nikon plan Apo 100×/NA 1.4 objective, a Nikon plan Fluor 20×/NA 0.5 objective, or a Nikon plan Fluor 40×/NA 0.75 objective and a Hamamatsu GRCA-ER camera (Hamamatsu Photonics) or a Zeiss AxioImager M2 fluorescence microscope equipped with an oil-immersion Zeiss plan Apo 100×/NA 1.4 objective and a Hamamatsu ORCA-R2 camera. Optical z-sections with 0.2 µm spacing were acquired using Volocity 6.3.1 software acquisition module (Perkin Elmer).

Image analysis

Images were deconvolved with an iterative restoration algorithm using calculated point spread functions and a confidence limit of 100% and an iteration limit of 30–35 using the Volocity restoration module (Perkin Elmer). Volocity software was used to adjust brightness and contrast and crop images. Images were adjusted for brightness and contrast and resized using Adobe Photoshop (Adobe). Figures were compiled in InkScape 0.91 or Adobe Illustrator 10.

To calculate the percentage of the PV population with internalized GFP-Rab foci, we viewed 3D reconstructed volumes of the optical z-slices and counted as positive any image that had at least one GFP focus inside the boundary of the TgGRA7 staining, which delineates the PVM.

Downloaded from http://rupress.org/jcb/article-pdf/216/12/4235/1597780/jcb_201701108.pdf by guest on 05 December 2025

To characterize the intra-PV GFP-Rab11A foci, we used fluorescence microscopy and the quantitation module of Volocity. First, using a Zeiss AxioImager M2 microscope, we acquired optical z-sections of infected cells with PVs containing 16 parasites to normalize the data for PV size and, hence, the developmental phase of the parasite. Then, we deconvolved the images and created a measurement protocol in Volocity, which measured objects in the 3D reconstructed volumes of the optical z-slices (Fig. S5). To identify the PV, we used two PV resident proteins with different localizations: soluble TgNTPase in the PV lumen and membrane-associated TgGRA7 in both the PVM and IVN. In the measurement protocol, the PV was pinpointed using the fluorescence intensity of TgGRA7 and TgNTPase; the thresholds of the intensity values were set manually by using the outer TgGRA7 PVM staining as the boundary of the PV. Next, the GFP-Rab11A foci were identified by fluorescence intensity (thresholds set manually such that the GFP-Rab11A puncta in the host cell were clearly delineated), and the GFP-Rab11A foci located within the boundary of the PV were highlighted. The measurement protocol consisted of the following steps: (1) find objects using fluorescence intensity with a minimum object size of 20 μm^3 for the TgGRA7 and TgNTPase channels; (2) combine the objects from the two channels and close with six iterations to create the item "PV"; (3) find objects using percent intensity for the GFP-Rab11A channel with a minimum object size of 0.1 μm^3, separate touching objects with an object size guide of 0.01 μm^3, and remove noise from objects with the fine filter; (4) find the intra-PV GFP-Rab11A foci by the "compartmentalize" function by "dividing items in GFP-Rab11A between items in the PV where sub-populations are inside"; and (5) measure the number of intra-PV GFP-Rab11A foci; the volume, shape factor, and distance to the PV centroid of the foci; and the volume and shape factor of the PV. The measurements were exported to Microsoft Excel, and means and SDs were calculated. The results were reported as percentage of the values calculated for RH parasites, the reference controls.

The level of colocalization was measured using Volocity. Fluorescent intensity thresholds were set by measuring, using an ROI, the fluorescence intensity of each channel in a region of the cell without staining for either signal (background). To compare the level of colocalization, PCCs and MOCs were calculated along with a positive product of the difference of the means channel, which was generated by calculating the product of the difference from the mean for each voxel.

To calculate the percent of the PV population with a PVM projection (PVMP), we viewed 3D reconstructed volumes of the optical z-slices and counted as positive any image where projections of the PVM, identified by immunostaining for TgGRA7, were observed extending into the host cell cytosol.

To calculate the percentage of the PV population with specific BODIPY TR C5-ceramide staining patterns, we categorized PVs according to the following characteristics: PVM, PV (patches, strand), PPM, and parasite organelle staining. The criteria for PVM staining are (1) the majority of the PVM is stained (100–80%), (2) staining of the PVM in large patches (80–10%), and (3) small patches or no discernible staining (10–0%). Two categories were identified for staining within the PV: (1) a concentration of staining within the PV in a patch-like structure, often near the edge of the PV (patches); and (2) a strand-like structure of staining connecting to the PVM, often observed connecting to PPM. The criteria for staining of the PPM are: (1) bright staining of the entire PPM of the majority of parasites (++), (2) less staining of the PPM (+), and (3) little to no discernible staining of the PPM (−). Staining of parasite organelles was categorized in a manner similar to PPM: (1) bright staining inside the parasites where the organelles are clearly identifiable (++), (2) some staining evident inside the parasite but the organelles are not clearly identifiable (+), and (3) no staining evident inside the parasites (−).

Transmission EM

For ultrastructural observations of *Toxoplasma*-infected cells by thin-section transmission EM, infected cells were fixed in 2.5% glutaraldehyde in 0.1 mM sodium cacodylate (EMS) and processed as described previously (Coppens and Joiner, 2003). Ultrathin sections of infected cells were stained before examination with a Philips CM120 EM under 80 kV. For immuno-EM of GFP-Rab11A, TgLCAT, and TgGRA7, *Toxoplasma*-infected cells were fixed in 4% paraformaldehyde (Electron Microscopy Sciences) in 0.25 M Hepes, pH 7.4, for 1 h at room temperature, then in 8% paraformaldehyde in the same buffer overnight at 4°C. They were infiltrated, frozen, and sectioned as previously described (Quittnat et al., 2004). The sections were immunolabeled with antibodies against GFP (1:10), TgLCAT (1:20), or TgGRA7 (1:100) diluted in PBS/1% fish skin gelatin, and then with secondary IgG antibodies coupled to various protein A–gold particle sizes (Department of Cell Biology, Medical School, Utrecht University, Utrecht, Netherlands).

CLEM

Thin carbon film grid patterns were imprinted onto 10-mm glass coverslips using a superimposed transmission EM (TEM) index grid during carbon evaporation. Coverslips were rinsed with 70% ethanol, treated with 0.1% poly-L-lysine for 30 min at room temperature, washed twice with PBS, and incubated overnight in a laminar flow hood under UV light. HeLa cells transiently expressing GFP-Rab1A were seeded to a well of a six-well plate and grown overnight in Alpha MEM medium. The cells were infected with *Toxoplasma* expressing RFP at a multiplicity of infection of 5 for 1 h at 37°C, washed four times with PBS, detached with trypsin, resuspended in Alpha MEM medium, and counted with a hemocytometer. Each polylysine-treated, gridded coverslip was seeded with 25,000 cells in Alpha MEM medium and incubated at 37°C for 29 h. Samples were washed twice with PBS, fixed with 4% EM-grade formaldehyde and 0.01% EM-grade glutaraldehyde (both from EMS) in PBS for 15 min, washed twice with PBS, incubated with 1 µg/ml DAPI for 5 min, washed twice with PBS, washed once with 0.2M carbonate-bicarbonate buffer, pH 9.1, and mounted with 50% glycerol containing DABCO (1,4-diazabicyclo [2,2,2]-octane). Samples were viewed with a Nikon plan Fluor 20×/NA 0.5 objective (to determine the placement of specific cells within the grid) and a Nikon plan Fluor 40×/NA 0.75 objective (to image specific cells by acquiring optical z-sections; Nikon 90i microscope). After light microscopy imaging, cells were fixed with 4% paraformaldehyde, 2% glutaraldehyde, and 2 mM $CaCl_2$ in Pipes buffer overnight, quenched with 50 mM glycine in Pipes buffer for 15 min, washed with Pipes buffer, and poststained sequentially with reduced osmium (1% osmium tetroxide containing 0.25% potassium ferrocyanide), 1% tannic acid, and 1% uranyl acetate (30 min each with water and washing in-between staining steps). After staining, cells on coverslips were dehydrated with serial graded ethanol from 30% to 100% at 10 min each and then infiltrated and embedded in Spurr's resin (EMS). Individual *Toxoplasma*-infected cells imaged by light microscopy before embedding were located via grid number. Serial ultrathin sections at ∼70 nm were collected using an ultramicrotome (UC6; Leica Microsystems). EM images of each serial section were taken using a Tecnai T12 transmission electron microscope (FEI) at 80 KeV and imaged using AMT digital camera. Image analysis and processing were done using Photoshop and Fiji.

Statistical analysis

Numerical data are presented as means ± SD or in box plots using Kaleidagraph software (version 4.1.3; Synergy Software). Whiskers of the box plots represent the upper and lower values excluding outliers,

Downloaded from http://rupress.org/jcb/article-pdf/216/12/4235/1597780/jcb_201701108.pdf by guest on 05 December 2025

outliers are marked as open circles, and the line inside the box is the median value. To compare samples to the control, we used either a student *t* test or one-way ANOVA with a Tukey's honest significant difference post-hoc test using Kaleidagraph software.

Online supplemental material

Fig. S1 shows the internalization into the *Toxoplasma* PV of host Rab GTPases involved in the endocytosis, recycling, retrograde, exocytosis, and autophagosomal pathways. Fig. S2 shows the PV internalization of endogenous multivesicular body markers and the lack of internalization of Ras and a Rab1 effector. Fig. S3 shows the correlation of light and EM images of infected HeLa cells expressing GFP-Rab1A. Fig. S4 shows the concentration of host GFP-Rab11A foci with the IVN-associated proteins TgGRA4 and TgGRA8, the localization of TgLCAT to the IVN, and the lack of a role of TgGRA7 in host GFP-Rab11A PV internalization. Fig. S5 details the measurement protocol used to measure the characteristics of intra-PV host GFP-Rab11A foci.

Acknowledgments

We thank the members of the Coppens' laboratory for helpful discussion during the course of this work. We are grateful to the generous providers of plasmids and antibodies used in this study. We also thank the excellent technical staff of the Electron Microscopy Core Facility at Yale School of Medicine, the Johns Hopkins University School of Medicine Microscopy Facility, and John Strong at the Electron Microscopy Core Imaging Facility of the University of Maryland.

This work used an EM sample preparation instrument that was purchased with funding from a National Institutes of Health Shared Instrumentation Grant (1S10RR26870-1) awarded to University of Maryland, Baltimore. The mouse monoclonal anti–LIMP/LAMP3/CD63 (H5C6) antibody developed by Thomas August and James E.K. Hildreth was obtained from the Developmental Studies Hybridoma Bank developed under the auspices of the Eunice Kennedy Shriver National Institute of Child Health and Human Development and maintained by the Department of Biology, The University of Iowa, Iowa City, IA. This study was supported by the National Institutes of Health (grant AI060767 to I. Coppens).

The authors declare no competing financial interests.

Author contributions: conceptualization, data curation, supervision, investigation, funding acquisition, project administration, visualization, and writing, J.D. Romano and I. Coppens; formal analysis, J.D. Romano, S.J. Nolan; methodology, J.D. Romano, S.J. Nolan, K. Ehrenman, C. Porter, E.J. Hartman, R.-c. Hsia, and I. Coppens; resources, R.-c. Hsia; validation, J.D. Romano, I. Coppens, and S.J. Nolan; editing, S.J. Nolan and E.J. Hartman.

Submitted: 16 January 2017
Revised: 28 July 2017
Accepted: 8 September 2017

References

Allan, B.B., B.D. Moyer, and W.E. Balch. 2000. Rab1 recruitment of p115 into a cis-SNARE complex: programming budding COPII vesicles for fusion. *Science.* 289:444–448. https://doi.org/10.1126/science.289.5478.444

Asrat, S., D.A. de Jesús, A.D. Hempstead, V. Ramabhadran, and R.R. Isberg. 2014. Bacterial pathogen manipulation of host membrane trafficking. *Annu. Rev. Cell Dev. Biol.* 30:79–109. https://doi.org/10.1146/annurev-cellbio-100913-013439

Babbey, C.M., N. Ahktar, E. Wang, C.C.-H. Chen, B.D. Grant, and K.W. Dunn. 2006. Rab10 regulates membrane transport through early endosomes of polarized Madin-Darby canine kidney cells. *Mol. Biol. Cell.* 17:3156–3175. https://doi.org/10.1091/mbc.E05-08-0799

Bampton, E.T.W., C.G. Goemans, D. Niranjan, N. Mizushima, and A.M. Tolkovsky. 2005. The dynamics of autophagy visualized in live cells: from autophagosome formation to fusion with endo/lysosomes. *Autophagy.* 1:23–36. https://doi.org/10.4161/auto.1.1.1495

Barber, J., A.J. Trees, M. Owen, and B. Tennant. 1993. Isolation of *Neospora caninum* from a British dog. *Vet. Rec.* 133:531–532. https://doi.org/10.1136/vr.133.21.531

Barbero, P., L. Bittova, and S.R. Pfeffer. 2002. Visualization of Rab9-mediated vesicle transport from endosomes to the trans-Golgi in living cells. *J. Cell Biol.* 156:511–518. https://doi.org/10.1083/jcb.200109030

Beard, M., A. Satoh, J. Shorter, and G. Warren. 2005. A cryptic Rab1-binding site in the p115 tethering protein. *J. Biol. Chem.* 280:25840–25848. https://doi.org/10.1074/jbc.M503925200

Blader, I.J., and A.A. Koshy. 2014. *Toxoplasma gondii* development of its replicative niche: in its host cell and beyond. *Eukaryot. Cell.* 13:965–976. https://doi.org/10.1128/EC.00081-14

Bucci, C., R.G. Parton, I.H. Mather, H. Stunnenberg, K. Simons, B. Hoflack, and M. Zerial. 1992. The small GTPase rab5 functions as a regulatory factor in the early endocytic pathway. *Cell.* 70:715–728. https://doi.org/10.1016/0092-8674(92)90306-W

Butterworth, M.B., R.S. Edinger, M.R. Silvis, L.I. Gallo, X. Liang, G. Apodaca, R.A. Frizzell, and J.P. Johnson. 2012. Rab11b regulates the trafficking and recycling of the epithelial sodium channel (ENaC). *Am. J. Physiol. Renal Physiol.* 302:F581–F590. https://doi.org/10.1152/ajprenal.00304.2011

Caffaro, C.E., and J.C. Boothroyd. 2011. Evidence for host cells as the major contributor of lipids in the intravacuolar network of *Toxoplasma*-infected cells. *Eukaryot. Cell.* 10:1095–1099. https://doi.org/10.1128/EC.00002-11

Cebrian, I., C. Croce, N.A. Guerrero, N. Blanchard, and L.S. Mayorga. 2016. Rab22a controls MHC-I intracellular trafficking and antigen cross-presentation by dendritic cells. *EMBO Rep.* 17:1753–1765. https://doi.org/10.15252/embr.201642358

Cesbron-Delauw, M.-F., C. Gendrin, L. Travier, P. Ruffiot, and C. Mercier. 2008. Apicomplexa in mammalian cells: trafficking to the parasitophorous vacuole. *Traffic.* 9:657–664. https://doi.org/10.1111/j.1600-0854.2008.00728.x

Chen, Y., and J. Lippincott-Schwartz. 2013. Rab10 delivers GLUT4 storage vesicles to the plasma membrane. *Commun. Integr. Biol.* 6:e23779. https://doi.org/10.4161/cib.23779

Chen, W., Y. Feng, D. Chen, and A. Wandinger-Ness. 1998. Rab11 is required for trans-golgi network-to-plasma membrane transport and a preferential target for GDP dissociation inhibitor. *Mol. Biol. Cell.* 9:3241–3257. https://doi.org/10.1091/mbc.9.11.3241

Clough, B., and E.-M. Frickel. 2017. The *Toxoplasma* Parasitophorous Vacuole: An Evolving Host-Parasite Frontier. *Trends Parasitol.* 33:473–488. https://doi.org/10.1016/j.pt.2017.02.007

Coppens, I. 2014. Exploitation of auxotrophies and metabolic defects in Toxoplasma as therapeutic approaches. *Int. J. Parasitol.* 44:109–120. https://doi.org/10.1016/j.ijpara.2013.09.003

Coppens, I., and K.A. Joiner. 2003. Host but not parasite cholesterol controls *Toxoplasma* cell entry by modulating organelle discharge. *Mol. Biol. Cell.* 14:3804–3820. https://doi.org/10.1091/mbc.E02-12-0830

Coppens, I., F.R. Opperdoes, P.J. Courtoy, and P. Baudhuin. 1987. Receptor-mediated endocytosis in the bloodstream form of *Trypanosoma brucei*. *J. Protozool.* 34:465–473. https://doi.org/10.1111/j.1550-7408.1987.tb03216.x

Coppens, I., J.D. Dunn, J.D. Romano, M. Pypaert, H. Zhang, J.C. Boothroyd, and K.A. Joiner. 2006. *Toxoplasma gondii* sequesters lysosomes from mammalian hosts in the vacuolar space. *Cell.* 125:261–274. https://doi.org/10.1016/j.cell.2006.01.056

Daro, E., P. van der Sluijs, T. Galli, and I. Mellman. 1996. Rab4 and cellubrevin define different early endosome populations on the pathway of transferrin receptor recycling. *Proc. Natl. Acad. Sci. USA.* 93:9559–9564. https://doi.org/10.1073/pnas.93.18.9559

Dejgaard, S.Y., A. Murshid, A. Erman, O. Kizilay, D. Verbich, R. Lodge, K. Dejgaard, T.B.N. Ly-Hartig, R. Pepperkok, J.C. Simpson, and J.F. Presley. 2008. Rab18 and Rab43 have key roles in ER-Golgi trafficking. *J. Cell Sci.* 121:2768–2781. https://doi.org/10.1242/jcs.021808

de Melo, E.J., and W. de Souza. 1996. Pathway of C6-NBD-Ceramide on the host cell infected with Toxoplasma gondii. *Cell Struct. Funct.* 21:47–52. https://doi.org/10.1247/csf.21.47

de Melo, E.J., T.U. de Carvalho, and W. de Souza. 1992. Penetration of Toxoplasma gondii into host cells induces changes in the distribution of the mitochondria and the endoplasmic reticulum. *Cell Struct. Funct.* 17:311–317. https://doi.org/10.1247/csf.17.311

Downloaded from http://rupress.org/jcb/article-pdf/216/12/4235/1597780/jcb_201701108.pdf by guest on 05 December 2025

Derré, I., R. Swiss, and H. Agaisse. 2011. The lipid transfer protein CERT interacts with the Chlamydia inclusion protein IncD and participates to ER-Chlamydia inclusion membrane contact sites. *PLoS Pathog.* 7:e1002092. https://doi.org/10.1371/journal.ppat.1002092

de Souza, W., and M. Attias. 2015. New views of the Toxoplasma gondii parasitophorous vacuole as revealed by Helium Ion Microscopy (HIM). *J. Struct. Biol.* 191:76–85. https://doi.org/10.1016/j.jsb.2015.05.003

Dou, Z., I. Coppens, and V.B. Carruthers. 2013. Non-canonical maturation of two papain-family proteases in *Toxoplasma gondii*. *J. Biol. Chem.* 288:3523–3534. https://doi.org/10.1074/jbc.M112.443697

Dou, Z., O.L. McGovern, M. Di Cristina, and V.B. Carruthers. 2014. *Toxoplasma gondii* ingests and digests host cytosolic proteins. *MBio.* 5:e01188–e14. https://doi.org/10.1128/mBio.01188-14

Dubremetz, J.F., A. Achbarou, D. Bermudes, and K.A. Joiner. 1993. Kinetics and pattern of organelle exocytosis during Toxoplasma gondii/host-cell interaction. *Parasitol. Res.* 79:402–408. https://doi.org/10.1007/BF00931830

Dzierszinski, F., M. Nishi, L. Ouko, and D.S. Roos. 2004. Dynamics of Toxoplasma gondii differentiation. *Eukaryot. Cell.* 3:992–1003. https://doi.org/10.1128/EC.3.4.992-1003.2004

English, A.R., and G.K. Voeltz. 2013. Rab10 GTPase regulates ER dynamics and morphology. *Nat. Cell Biol.* 15:169–178. https://doi.org/10.1038/ncb2647

Feng, Y., B. Press, and A. Wandinger-Ness. 1995. Rab 7: an important regulator of late endocytic membrane traffic. *J. Cell Biol.* 131:1435–1452. https://doi.org/10.1083/jcb.131.6.1435

Girod, A., B. Storrie, J.C. Simpson, L. Johannes, B. Goud, L.M. Roberts, J.M. Lord, T. Nilsson, and R. Pepperkok. 1999. Evidence for a COP-I-independent transport route from the Golgi complex to the endoplasmic reticulum. *Nat. Cell Biol.* 1:423–430. https://doi.org/10.1038/15658

Gold, D.A., A.D. Kaplan, A. Lis, G.C.L. Bett, E.E. Rosowski, K.M. Cirelli, A. Bougdour, S.M. Sidik, J.R. Beck, S. Lourido, et al. 2015. The Toxoplasma Dense Granule Proteins GRA17 and GRA23 Mediate the Movement of Small Molecules between the Host and the Parasitophorous Vacuole. *Cell Host Microbe.* 17:642–652. https://doi.org/10.1016/j.chom.2015.04.003

Gorvel, J.P., P. Chavrier, M. Zerial, and J. Gruenberg. 1991. rab5 controls early endosome fusion in vitro. *Cell.* 64:915–925. https://doi.org/10.1016/0092-8674(91)90316-Q

Haas, A.K., S. Yoshimura, D.J. Stephens, C. Preisinger, E. Fuchs, and F.A. Barr. 2007. Analysis of GTPase-activating proteins: Rab1 and Rab43 are key Rabs required to maintain a functional Golgi complex in human cells. *J. Cell Sci.* 120:2997–3010. https://doi.org/10.1242/jcs.014225

Hakimi, M.-A., P. Olias, and L.D. Sibley. 2017. Toxoplasma Effectors Targeting Host Signaling and Transcription. *Clin. Microbiol. Rev.* 30:615–645. https://doi.org/10.1128/CMR.00005-17

Horgan, C.P., M. Walsh, T.H. Zurawski, and M.W. McCaffrey. 2004. Rab11-FIP3 localises to a Rab11-positive pericentrosomal compartment during interphase and to the cleavage furrow during cytokinesis. *Biochem. Biophys. Res. Commun.* 319:83–94. https://doi.org/10.1016/j.bbrc.2004.04.157

Jacobs, D., J.F. Dubremetz, A. Loyens, F. Bosman, and E. Saman. 1998. Identification and heterologous expression of a new dense granule protein (GRA7) from Toxoplasma gondii. *Mol. Biochem. Parasitol.* 91:237–249. https://doi.org/10.1016/S0166-6851(97)00204-1

Junutula, J.R., A.M. De Maziére, A.A. Peden, K.E. Ervin, R.J. Advani, S.M. van Dijk, J. Klumperman, and R.H. Scheller. 2004. Rab14 is involved in membrane trafficking between the Golgi complex and endosomes. *Mol. Biol. Cell.* 15:2218–2229. https://doi.org/10.1091/mbc.E03-10-0777

Kagan, J.C., and C.R. Roy. 2002. Legionella phagosomes intercept vesicular traffic from endoplasmic reticulum exit sites. *Nat. Cell Biol.* 4:945–954. https://doi.org/10.1038/ncb883

Kagan, J.C., M.-P. Stein, M. Pypaert, and C.R. Roy. 2004. Legionella subvert the functions of Rab1 and Sec22b to create a replicative organelle. *J. Exp. Med.* 199:1201–1211. https://doi.org/10.1084/jem.20031706

Kelly, E.E., F. Giordano, C.P. Horgan, F. Jollivet, G. Raposo, and M.W. McCaffrey. 2012. Rab30 is required for the morphological integrity of the Golgi apparatus. *Biol. Cell.* 104:84–101. https://doi.org/10.1111/boc.201100080

Kitt, K.N., D. Hernández-Deviez, S.D. Ballantyne, E.T. Spiliotis, J.E. Casanova, and J.M. Wilson. 2008. Rab14 regulates apical targeting in polarized epithelial cells. *Traffic.* 9:1218–1231. https://doi.org/10.1111/j.1600-0854.2008.00752.x

Kobayashi, T., E. Stang, K.S. Fang, P. de Moerloose, R.G. Parton, and J. Gruenberg. 1998. A lipid associated with the antiphospholipid syndrome regulates endosome structure and function. *Nature.* 392:193–197. https://doi.org/10.1038/32440

Kobayashi, T., U.M. Vischer, C. Rosnoblet, C. Lebrand, M. Lindsay, R.G. Parton, E.K. Kruithof, and J. Gruenberg. 2000. The tetraspanin CD63/lamp3 cycles between endocytic and secretory compartments in human endothelial cells. *Mol. Biol. Cell.* 11:1829–1843. https://doi.org/10.1091/mbc.11.5.1829

Larson, E.T., F. Parussini, M.-H. Huynh, J.D. Giebel, A.M. Kelley, L. Zhang, M. Bogyo, E.A. Merritt, and V.B. Carruthers. 2009. Toxoplasma gondii cathepsin L is the primary target of the invasion-inhibitory compound morpholinurea-leucyl-homophenyl-vinyl sulfone phenyl. *J. Biol. Chem.* 284:26839–26850. https://doi.org/10.1074/jbc.M109.003780

Lombardi, D., T. Soldati, M.A. Riederer, Y. Goda, M. Zerial, and S.R. Pfeffer. 1993. Rab9 functions in transport between late endosomes and the trans Golgi network. *EMBO J.* 12:677–682.

Mallard, F., B.L. Tang, T. Galli, D. Tenza, A. Saint-Pol, X. Yue, C. Antony, W. Hong, B. Goud, and L. Johannes. 2002. Early/recycling endosomes-to-TGN transport involves two SNARE complexes and a Rab6 isoform. *J. Cell Biol.* 156:653–664. https://doi.org/10.1083/jcb.200110081

Martinez, O., A. Schmidt, J. Salaméro, B. Hoflack, M. Roa, and B. Goud. 1994. The small GTP-binding protein rab6 functions in intra-Golgi transport. *J. Cell Biol.* 127:1575–1588. https://doi.org/10.1083/jcb.127.6.1575

McCaffrey, M.W., A. Bielli, G. Cantalupo, S. Mora, V. Roberti, M. Santillo, F. Drummond, and C. Bucci. 2001. Rab4 affects both recycling and degradative endosomal trafficking. *FEBS Lett.* 495:21–30. https://doi.org/10.1016/S0014-5793(01)02359-6

Melo, E.J., and W. de Souza. 1997. Relationship between the host cell endoplasmic reticulum and the parasitophorous vacuole containing Toxoplasma gondii. *Cell Struct. Funct.* 22:317–323. https://doi.org/10.1247/csf.22.317

Melo, E.J., T.M. Carvalho, and W. De Souza. 2001. Behaviour of microtubules in cells infected with *Toxoplasma gondii*. *Biocell.* 25:53–59.

Mercier, C., D.K. Howe, D. Mordue, M. Lingnau, and L.D. Sibley. 1998. Targeted disruption of the GRA2 locus in Toxoplasma gondii decreases acute virulence in mice. *Infect. Immun.* 66:4176–4182.

Mercier, C., J.-F. Dubremetz, B. Rauscher, L. Lecordier, L.D. Sibley, and M.-F. Cesbron-Delauw. 2002. Biogenesis of nanotubular network in Toxoplasma parasitophorous vacuole induced by parasite proteins. *Mol. Biol. Cell.* 13:2397–2409. https://doi.org/10.1091/mbc.E02-01-0021

Méresse, S., J.P. Gorvel, and P. Chavrier. 1995. The rab7 GTPase resides on a vesicular compartment connected to lysosomes. *J. Cell Sci.* 108:3349–3358.

Militello, R.D., D.B. Munafó, W. Berón, L.A. López, S. Monier, B. Goud, and M.I. Colombo. 2013. Rab24 is required for normal cell division. *Traffic.* 14:502–518. https://doi.org/10.1111/tra.12057

Moyer, B.D., B.B. Allan, and W.E. Balch. 2001. Rab1 interaction with a GM130 effector complex regulates COPII vesicle cis--Golgi tethering. *Traffic.* 2:268–276. https://doi.org/10.1034/j.1600-0854.2001.1o007.x

Munafó, D.B., and M.I. Colombo. 2002. Induction of autophagy causes dramatic changes in the subcellular distribution of GFP-Rab24. *Traffic.* 3:472–482. https://doi.org/10.1034/j.1600-0854.2002.30704.x

Nolan, S.J., J.D. Romano, T. Luechtefeld, and I. Coppens. 2015. *Neospora caninum* Recruits Host Cell Structures to Its Parasitophorous Vacuole and Salvages Lipids from Organelles. *Eukaryot. Cell.* 14:454–473. https://doi.org/10.1128/EC.00262-14

Nolan, S.J., J.D. Romano, and I. Coppens. 2017. Host lipid droplets: An important source of lipids salvaged by the intracellular parasite *Toxoplasma gondii*. *PLoS Pathog.* 13:e1006362. https://doi.org/10.1371/journal.ppat.1006362

Parussini, F., I. Coppens, P.P. Shah, S.L. Diamond, and V.B. Carruthers. 2010. Cathepsin L occupies a vacuolar compartment and is a protein maturase within the endo/exocytic system of *Toxoplasma* gondii. *Mol. Microbiol.* 76:1340–1357. https://doi.org/10.1111/j.1365-2958.2010.07181.x

Pernas, L., and J.C. Boothroyd. 2010. Association of host mitochondria with the parasitophorous vacuole during Toxoplasma infection is not dependent on rhoptry proteins ROP2/8. *Int. J. Parasitol.* 40:1367–1371. https://doi.org/10.1016/j.ijpara.2010.07.002

Pernas, L., Y. Adomako-Ankomah, A.J. Shastri, S.E. Ewald, M. Treeck, J.P. Boyle, and J.C. Boothroyd. 2014. Toxoplasma effector MAF1 mediates recruitment of host mitochondria and impacts the host response. *PLoS Biol.* 12:e1001845. https://doi.org/10.1371/journal.pbio.1001845

Plutner, H., A.D. Cox, S. Pind, R. Khosravi-Far, J.R. Bourne, R. Schwaninger, C.J. Der, and W.E. Balch. 1991. Rab1b regulates vesicular transport between the endoplasmic reticulum and successive Golgi compartments. *J. Cell Biol.* 115:31–43. https://doi.org/10.1083/jcb.115.1.31

Press, B., Y. Feng, B. Hoflack, and A. Wandinger-Ness. 1998. Mutant Rab7 causes the accumulation of cathepsin D and cation-independent mannose 6-phosphate receptor in an early endocytic compartment. *J. Cell Biol.* 140:1075–1089. https://doi.org/10.1083/jcb.140.5.1075

Downloaded from http://rupress.org/jcb/article-pdf/216/12/4235/1597780/jcb_201701108.pdf by guest on 05 December 2025

Pszenny, V., K. Ehrenman, J.D. Romano, A. Kennard, A. Schultz, D.S. Roos, M.E. Grigg, V.B. Carruthers, and I. Coppens. 2016. A Lipolytic Lecithin :Cholesterol Acyltransferase Secreted by *Toxoplasma* Facilitates Parasite Replication and Egress. *J. Biol. Chem.* 291:3725–3746. https://doi.org/10.1074/jbc.M115.671974

Quittnat, F., Y. Nishikawa, T.T. Stedman, D.R. Voelker, J.-Y. Choi, M.M. Zahn, R.C. Murphy, R.M. Barkley, M. Pypaert, K.A. Joiner, and I. Coppens. 2004. On the biogenesis of lipid bodies in ancient eukaryotes: synthesis of triacylglycerols by a *Toxoplasma* DGAT1-related enzyme. *Mol. Biochem. Parasitol.* 138:107–122. https://doi.org/10.1016/j.molbiopara.2004.08.004

Ren, M., G. Xu, J. Zeng, C. De Lemos-Chiarandini, M. Adesnik, and D.D. Sabatini. 1998. Hydrolysis of GTP on rab11 is required for the direct delivery of transferrin from the pericentriolar recycling compartment to the cell surface but not from sorting endosomes. *Proc. Natl. Acad. Sci. USA.* 95:6187–6192. https://doi.org/10.1073/pnas.95.11.6187

Riederer, M.A., T. Soldati, A.D. Shapiro, J. Lin, and S.R. Pfeffer. 1994. Lysosome biogenesis requires Rab9 function and receptor recycling from endosomes to the trans-Golgi network. *J. Cell Biol.* 125:573–582. https://doi.org/10.1083/jcb.125.3.573

Romano, J.D., N. Bano, and I. Coppens. 2008. New host nuclear functions are not required for the modifications of the parasitophorous vacuole of *Toxoplasma. Cell. Microbiol.* 10:465–476.

Romano, J.D., S. Sonda, E. Bergbower, M.E. Smith, and I. Coppens. 2013. *Toxoplasma gondii* salvages sphingolipids from the host Golgi through the rerouting of selected Rab vesicles to the parasitophorous vacuole. *Mol. Biol. Cell.* 24:1974–1995. https://doi.org/10.1091/mbc.E12-11-0827

Rome, M.E., J.R. Beck, J.M. Turetzky, P. Webster, and P.J. Bradley. 2008. Intervacuolar transport and unique topology of GRA14, a novel dense granule protein in Toxoplasma gondii. *Infect. Immun.* 76:4865–4875. https://doi.org/10.1128/IAI.00782-08

Rommereim, L.M., V. Bellini, B.A. Fox, G. Pètre, C. Rak, B. Touquet, D. Aldebert, J.-F. Dubremetz, M.-F. Cesbron-Delauw, C. Mercier, and D.J. Bzik. 2016. Phenotypes Associated with Knockouts of Eight Dense Granule Gene Loci (GRA2-9) in Virulent *Toxoplasma gondii. PLoS One.* 11:e0159306–e0159321. https://doi.org/10.1371/journal.pone.0159306

Roos, D.S., R.G. Donald, N.S. Morrissette, and A.L. Moulton. 1994. Molecular tools for genetic dissection of the protozoan parasite Toxoplasma gondii. *Methods Cell Biol.* 45:27–63. https://doi.org/10.1016/S0091-679X(08)61845-2

Rzomp, K.A., L.D. Scholtes, B.J. Briggs, G.R. Whittaker, and M.A. Scidmore. 2003. Rab GTPases are recruited to chlamydial inclusions in both a species-dependent and species-independent manner. *Infect. Immun.* 71:5855–5870. https://doi.org/10.1128/IAI.71.10.5855-5870.2003

Saka, H.A., and R.H. Valdivia. 2010. Acquisition of nutrients by Chlamydiae: unique challenges of living in an intracellular compartment. *Curr. Opin. Microbiol.* 13:4–10. https://doi.org/10.1016/j.mib.2009.11.002

Sannerud, R., M. Marie, C. Nizak, H.A. Dale, K. Pernet-Gallay, F. Perez, B. Goud, and J. Saraste. 2006. Rab1 defines a novel pathway connecting the pre-Golgi intermediate compartment with the cell periphery. *Mol. Biol. Cell.* 17:1514–1526. https://doi.org/10.1091/mbc.E05-08-0792

Sano, H., L. Eguez, M.N. Teruel, M. Fukuda, T.D. Chuang, J.A. Chavez, G.E. Lienhard, and T.E. McGraw. 2007. Rab10, a target of the AS160 Rab GAP, is required for insulin-stimulated translocation of GLUT4 to the adipocyte plasma membrane. *Cell Metab.* 5:293–303. https://doi.org/10.1016/j.cmet.2007.03.001

Sano, H., W.G. Roach, G.R. Peck, M. Fukuda, and G.E. Lienhard. 2008. Rab10 in insulin-stimulated GLUT4 translocation. *Biochem. J.* 411:89–95. https://doi.org/10.1042/BJ20071318

Saraste, J. 2016. Spatial and Functional Aspects of ER-Golgi Rabs and Tethers. *Front. Cell Dev. Biol.* 4:28. https://doi.org/10.3389/fcell.2016.00028

Schlierf, B., G.H. Fey, J. Hauber, G.M. Hocke, and O. Rosorius. 2000. Rab11b is essential for recycling of transferrin to the plasma membrane. *Exp. Cell Res.* 259:257–265. https://doi.org/10.1006/excr.2000.4947

Schuck, S., M.J. Gerl, A. Ang, A. Manninen, P. Keller, I. Mellman, and K. Simons. 2007. Rab10 is involved in basolateral transport in polarized Madin-Darby canine kidney cells. *Traffic.* 8:47–60. https://doi.org/10.1111/j.1600-0854.2006.00506.x

Schwab, J.C., C.J. Beckers, and K.A. Joiner. 1994. The parasitophorous vacuole membrane surrounding intracellular Toxoplasma gondii functions as a molecular sieve. *Proc. Natl. Acad. Sci. USA.* 91:509–513. https://doi.org/10.1073/pnas.91.2.509

Sibley, L.D. 2011. Invasion and intracellular survival by protozoan parasites. *Immunol. Rev.* 240:72–91. https://doi.org/10.1111/j.1600-065X.2010.00990.x

Sibley, L.D., I.R. Niesman, S.F. Parmley, and M.F. Cesbron-Delauw. 1995. Regulated secretion of multi-lamellar vesicles leads to formation of a tubulo-vesicular network in host-cell vacuoles occupied by Toxoplasma gondii. *J. Cell Sci.* 108:1669–1677.

Silvis, M.R., C.A. Bertrand, N. Ameen, F. Golin-Bisello, M.B. Butterworth, R.A. Frizzell, and N.A. Bradbury. 2009. Rab11b regulates the apical recycling of the cystic fibrosis transmembrane conductance regulator in polarized intestinal epithelial cells. *Mol. Biol. Cell.* 20:2337–2350. https://doi.org/10.1091/mbc.E08-01-0084

Sinai, A.P., P. Webster, and K.A. Joiner. 1997. Association of host cell endoplasmic reticulum and mitochondria with the Toxoplasma gondii parasitophorous vacuole membrane: a high affinity interaction. *J. Cell Sci.* 110:2117–2128.

Stenmark, H., R.G. Parton, O. Steele-Mortimer, A. Lütcke, J. Gruenberg, and M. Zerial. 1994. Inhibition of rab5 GTPase activity stimulates membrane fusion in endocytosis. *EMBO J.* 13:1287–1296.

Tisdale, E.J. 1999. A Rab2 mutant with impaired GTPase activity stimulates vesicle formation from pre-Golgi intermediates. *Mol. Biol. Cell.* 10:1837–1849. https://doi.org/10.1091/mbc.10.6.1837

Tisdale, E.J., and W.E. Balch. 1996. Rab2 is essential for the maturation of pre-Golgi intermediates. *J. Biol. Chem.* 271:29372–29379. https://doi.org/10.1074/jbc.271.46.29372

Tisdale, E.J., J.R. Bourne, R. Khosravi-Far, C.J. Der, and W.E. Balch. 1992. GTP-binding mutants of rab1 and rab2 are potent inhibitors of vesicular transport from the endoplasmic reticulum to the Golgi complex. *J. Cell Biol.* 119:749–761. https://doi.org/10.1083/jcb.119.4.749

Travier, L., R. Mondragon, J.-F. Dubremetz, K. Musset, M. Mondragon, S. Gonzalez, M.-F. Cesbron-Delauw, and C. Mercier. 2008. Functional domains of the Toxoplasma GRA2 protein in the formation of the membranous nanotubular network of the parasitophorous vacuole. *Int. J. Parasitol.* 38:757–773. https://doi.org/10.1016/j.ijpara.2007.10.010

Ullrich, O., S. Reinsch, S. Urbé, M. Zerial, and R.G. Parton. 1996. Rab11 regulates recycling through the pericentriolar recycling endosome. *J. Cell Biol.* 135:913–924. https://doi.org/10.1083/jcb.135.4.913

van der Sluijs, P., M. Hull, P. Webster, P. Mâle, B. Goud, and I. Mellman. 1992. The small GTP-binding protein rab4 controls an early sorting event on the endocytic pathway. *Cell.* 70:729–740. https://doi.org/10.1016/0092-8674(92)90307-X

Vitelli, R., M. Santillo, D. Lattero, M. Chiariello, M. Bifulco, C.B. Bruni, and C. Bucci. 1997. Role of the small GTPase Rab7 in the late endocytic pathway. *J. Biol. Chem.* 272:4391–4397. https://doi.org/10.1074/jbc.272.7.4391

Vollenweider, P., S.S. Martin, T. Haruta, A.J. Morris, J.G. Nelson, M. Cormont, Y. Le Marchand-Brustel, D.W. Rose, and J.M. Olefsky. 1997. The small guanosine triphosphate-binding protein Rab4 is involved in insulin-induced GLUT4 translocation and actin filament rearrangement in 3T3-L1 cells. *Endocrinology.* 138:4941–4949. https://doi.org/10.1210/endo.138.11.5493

Walker, M.E., E.E. Hjort, S.S. Smith, A. Tripathi, J.E. Hornick, E.H. Hinchcliffe, W. Archer, and K.M. Hager. 2008. Toxoplasma gondii actively remodels the microtubule network in host cells. *Microbes Infect.* 10:1440–1449. https://doi.org/10.1016/j.micinf.2008.08.014

Wang, D., J. Lou, C. Ouyang, W. Chen, Y. Liu, X. Liu, X. Cao, J. Wang, and L. Lu. 2010. Ras-related protein Rab10 facilitates TLR4 signaling by promoting replenishment of TLR4 onto the plasma membrane. *Proc. Natl. Acad. Sci. USA.* 107:13806–13811. https://doi.org/10.1073/pnas.1009428107

White, J., L. Johannes, F. Mallard, A. Girod, S. Grill, S. Reinsch, P. Keller, B. Tzschaschel, A. Echard, B. Goud, and E.H. Stelzer. 1999. Rab6 coordinates a novel Golgi to ER retrograde transport pathway in live cells. *J. Cell Biol.* 147:743–760. https://doi.org/10.1083/jcb.147.4.743

Wilcke, M., L. Johannes, T. Galli, V. Mayau, B. Goud, and J. Salamero. 2000. Rab11 regulates the compartmentalization of early endosomes required for efficient transport from early endosomes to the trans-golgi network. *J. Cell Biol.* 151:1207–1220. https://doi.org/10.1083/jcb.151.6.1207

Wilson, B.S., C. Nuoffer, J.L. Meinkoth, M. McCaffery, J.R. Feramisco, W.E. Balch, and M.G. Farquhar. 1994. A Rab1 mutant affecting guanine nucleotide exchange promotes disassembly of the Golgi apparatus. *J. Cell Biol.* 125:557–571. https://doi.org/10.1083/jcb.125.3.557

Wilson, G.M., A.B. Fielding, G.C. Simon, X. Yu, P.D. Andrews, R.S. Hames, A.M. Frey, A.A. Peden, G.W. Gould, and R. Prekeris. 2005. The FIP3-Rab11 protein complex regulates recycling endosome targeting to the cleavage furrow during late cytokinesis. *Mol. Biol. Cell.* 16:849–860. https://doi.org/10.1091/mbc.E04-10-0927

Ylä-Anttila, P., E. Mikkonen, K.E. Happonen, P. Holland, T. Ueno, A. Simonsen, and E.-L. Eskelinen. 2015. RAB24 facilitates clearance of autophagic compartments during basal conditions. *Autophagy.* 11:1833–1848. https://doi.org/10.1080/15548627.2015.1086522

Young, H.E., and A.C. Black Jr. 2004. Adult stem cells. *Anat. Rec. A Discov. Mol. Cell. Evol. Biol.* 276:75–102. https://doi.org/10.1002/ar.a.10134

Zhen, Y., and H. Stenmark. 2015. Cellular functions of Rab GTPases at a glance. *J. Cell Sci.* 128:3171–3176. https://doi.org/10.1242/jcs.166074

Downloaded from http://rupress.org/jcb/article-pdf/216/12/4235/1597780/jcb_201701108.pdf by guest on 05 December 2025